PULSAR POLAR CAP HEATING AND SURFACE THERMAL X-RAY EMISSION. II. INVERSE COMPTON RADIATION PAIR FRONTS

ALICE K. HARDING[1] AND ALEXANDER G. MUSLIMOV[2]

ABSTRACT

We investigate the production of electron-positron pairs by inverse Compton scattered (ICS) photons above a pulsar polar cap (PC) and calculate surface heating by returning positrons. This paper is a continuation of our self-consistent treatment of acceleration, pair dynamics, and electric field screening above pulsar PCs. We calculate the altitude of the inverse Compton pair-formation fronts, the flux of returning positrons, and present the heating efficiencies and X-ray luminosities. We revise pulsar death lines implying cessation of pair formation, and present them in surface magnetic field–period space. We find that virtually all known radio pulsars are capable of producing pairs by resonant and nonresonant ICS photons radiated by particles accelerated above the PC in a pure star-centered dipole field, so that our ICS pair death line coincides with empirical radio pulsar death. Our calculations show that ICS pairs are able to screen the accelerating electric field only for high PC surface temperatures and magnetic fields. We argue that such screening at ICS pair fronts occurs locally, slowing but not turning off acceleration of particles until screening can occur at a curvature radiation (CR) pair front at higher altitude. In the case where no screening occurs above the PC surface, we anticipate that the pulsar γ-ray luminosity will be a substantial fraction of its spin-down luminosity. The X-ray luminosity resulting from PC heating by ICS pair fronts is significantly lower than the PC heating luminosity from CR pair fronts, which dominates for most pulsars. PC heating from ICS pair fronts is highest in millisecond pulsars, which cannot produce CR pairs, and may account for observed thermal X-ray components in the spectra of these old pulsars.

Subject headings: pulsars: general — radiation mechanisms: nonthermal — relativity — stars: neutron — X-rays: stars

1. INTRODUCTION

In the last several years, the basic model of particle acceleration above a pulsar polar cap (PC) has been undergoing significant revision. Sturrock (1971), Ruderman & Sutherland (1975), and Arons & Scharlemann (1979) originally proposed that particles are accelerated by an induced electric field, producing curvature radiation (CR) photons which create electron-positron pairs in the strong magnetic field. The pairs short out the electric field above a pair-formation front (PFF), self-limiting the acceleration. In the process of screening or shorting-out the electric field, some fraction of the positrons are accelerated back toward the PCs and heat the surface of the neutron star (NS), producing a potentially observable X-ray emission component (Arons 1981). Two recent developments have introduced important changes to this picture. First was the finding of Muslimov & Tsygan (1992) that the effect of inertial-frame dragging near the NS surface greatly increases the induced electric field $E_{\parallel}$ above the PC in space-charge–limited flow models (Arons & Scharlemann 1979). The second was the realization that inverse Compton radiation of the primary particles can produce pairs that could potentially screen the electric field (Zhang et al. 1997; Harding & Muslimov 1998, hereafter HM98).

We have investigated the electric field screening and PC heating in the revised space-charge–limited flow (SCLF) model. In the first paper (Harding & Muslimov

2001, hereafter Paper I), we have presented our results for screening and PC heating by CR PFFs, as in Arons (1981), but using the frame-dragging electric field of Muslimov & Tsygan (1992). Paper I outlined a self-consistent calculation of the PFF height, returning positron flux and the screening scale length, where the $E_{\parallel}$ and the primary flux are adjusted for the change in charge density caused by the returning positrons. A main assumption of this calculation was that the screening scale is small compared to the height of the PFF, the location where the first pairs are produced. This turns out to be generally true for screening by CR-produced pairs, because the pair cascade multiplicity grows rapidly over small distances because of the strong dependence of CR photon energy on particle energy. Thus, the existence of a CR PFF always results in PC heating and full screening of $E_{\parallel}$. We found that the PC heating luminosity, as a fraction of the spin-down luminosity, increases with pulsar characteristic age, $\tau = P/2\dot{P}$, and should be detectable for pulsars with $\tau \gtrsim 10^6$ yr. The most significant heating occurs for pulsars near the death line for CR pair production, which is $\tau \sim 10^7$ yr for normal-period pulsars and $\tau \sim 10^8$ yr for millisecond pulsars. Our predicted X-ray luminosity due to PC heating is about a factor of 10 higher than the X-ray luminosity predicted by Arons (1981), because of the increase in accelerating voltage drop resulting from the inclusion of inertial-frame dragging effects. We also predicted that older pulsars should have higher PC surface temperatures from heating.

In this second paper (Paper II), we present results of our investigation of electric field screening and PC heating by inverse Compton scattering (ICS) radiation PFFs. We investigate PC heating by ICS-produced pairs in all pulsars,

[1] Laboratory for High Energy Astrophysics, NASA/Goddard Space Flight Center, Greenbelt, MD 20771.
[2] Emergent Information Technologies, Inc., Space Sciences Sector, Upper Marlboro, MD 20774.

including those that produce CR pairs. For the older pulsars that do not produce pairs through CR, PC heating by positrons from ICS cascades is especially important. Our treatment of the ICS PFFs closely follows that of HM98, where cyclotron-resonant and nonresonant scattering are considered as separate radiation components. HM98 found that the ICS PFFs are located much closer to the NS surface than are the CR PFFs, because primaries with Lorentz factor of only $\sim 10^4$–10^5 can produce pairs via ICS, whereas Lorentz factors of at least $\sim 10^7$ are required for production of pairs via CR. They also found that the ICS PFFs of positrons returning from the upper PFF occur at a significant distance above the surface, so it is possible that ICS pairs fronts are unstable if screening of $E_\parallel$ at the lower PFF occurs. However, HM98 did not determine whether the ICS pairs were capable of screening at either the upper or lower PFFs.

This paper will attempt to answer those questions with a calculation similar to that of Paper I. In § 2, we describe the acceleration model for this calculation. We use a solution for $E_\parallel$ from Poisson's equation that imposes an upper boundary condition requiring that $E_\parallel = 0$ at the location of screening (as in HM98), which differs from that of Paper I, which used a solution with no upper boundary. The solution with an upper boundary is more appropriate for screening at ICS PFFs that form close to the surface, where the screening scale is generally comparable to the PFF height. This solution is required here because pairs from ICS photons may screen $E_\parallel$ close to the NS surface. In this case the value of $E_\parallel$ is suppressed because of the proximity of the screening to the surface. Section 2 also presents a calculation of ICS PFF height and the location of a new ICS pair death line. We find that virtually all known pulsars can produce pairs by either resonant ICS (RICS) or nonresonant ICS (NRICS) in a pure dipole field. Hibschmann & Arons (2001, hereafter HA01) have recently taken a different approach to determining pulsar death lines including ICS-produced pairs. They define the PFF as the location where the pair multiplicity achieves that required for complete screening of the $E_\parallel$, whereas we define the PFF as the location where pair production begins (i.e., where the first pairs are produced). In the case of CR this distinction is minor, since the screening scale is small compared to the PFF height, but in the case of ICS the distinction is very important, since the screening scale is comparable to the PFF height. HA01 also assume that the pair multiplicity required for screening is determined by the difference between the actual charge and the Goldreich-Julian charge at a distance from the NS surface that is roughly equal to the PC radius, whereas in our calculation the charge density required for screening is determined by the charge deficit at the location of creation of pairs, which can be much smaller. With their more restrictive definition of the PFF, their death lines differ significantly from ours. In § 3, we give self-consistent solutions for the fraction of positrons returning to the PC and for the screening scale. We also explore the question of whether positrons returning from the upper PFF can screen $E_\parallel$ near the lower PFF close to the NS surface. The subject of pulsar pair death lines, i.e., which NSs are capable of pair production, will be discussed in § 4. In § 5, we present our calculations of PC heating luminosity due to returning positrons, giving both numerical and analytic estimates. A summary and conclusions, as well as a comparison of results from both Papers I and II, will be given in § 6.

2. THE ACCELERATION OF PRIMARIES AND ONSET OF PAIR FORMATION

2.1. Acceleration Model

In this paper we exploit the same model for charged-particle acceleration that is described in Paper I. Namely, in the acceleration region we use the appropriate solution for the electric field and potential presented in that paper. For example, for most ICS pair fronts, where the screening occurs over the length scale smaller than the PC size, we use our formulae (A7)–(A10) of Paper I, whereas in the screening region (see § 3.2 for details) for all cases we model the electric field by equation (26) of Paper I.

2.2. Altitudes of the Pair-Formation Fronts

2.2.1. Analytic Estimates

For our analytic estimates we use the same simplified expressions for the accelerating electric field (cf. eqs. [34] and [35] of Paper I),

$$E_{\parallel 6} = \frac{B_{12}}{P}\kappa_{0.15}\begin{cases} 1.3zP^{-1/2} & \text{unsaturated}, \\ 5 \times 10^{-3}P^{-1} & \text{saturated}, \end{cases} \quad (1)$$

where the upper expression corresponds to the unsaturated regime (rising part of the accelerating field), and the lower to the saturated regime (nearly constant accelerating field). Equation (1) assumes that $\xi = 0.5$ and $\cos\chi \approx 1$; $E_{\parallel 6} \equiv E_\parallel/10^6$ esu, $\kappa_{0.15} = \kappa/0.15$, $B_{12} = B_0/10^{12}$ G, and z is the altitude in units of stellar radius, where ξ is the magnetic colatitude in units of the PC half-angle, χ is the angle between the magnetic and spin axes, $E_\parallel$ is the component of the electric field parallel to the magnetic field, B_0 is the surface value of the magnetic field strength, and κ is the dimensionless general relativistic parameter originating from the frame-dragging effect and accounting for the stellar compactness and moment of inertia.

Note that throughout this paper in all practical formulae we assume that P is the dimensionless value of pulsar spin period measured in seconds. Also, in all our analytic estimates based on the above formula we discriminate between unsaturated and saturated regimes of acceleration, with the unsaturated and saturated regimes occurring where the characteristic altitude of pair formation is respectively smaller or larger than the PC radius. The formal criteria corresponding to these regimes, e.g., in the B-P diagram, depend on the radiation mechanism for pair-producing photons and can be derived from the conditions $\zeta_* \lesssim 1$ and $\zeta_* \gtrsim 1$ for unsaturated and saturated regimes, respectively, where ζ_* is the characteristic altitude of screening scaled by the PC radius (see eqs. [36]–[38] below). These criteria translate into

$$P \lesssim P_*, \quad \text{unsaturated regime} \quad (2)$$

and

$$P \gtrsim P_*, \quad \text{saturated regime}, \quad (3)$$

where P_* is defined as, for curvature radiation,

$$P_*^{(CR)} = 0.1B_{12}^{4/9}. \quad (4)$$

Before we present P_* for the ICS case, note that for the physical conditions we discuss in this paper it is conven-

ient (especially in our analytic calculations) to treat the ICS photons as generated via two different regimes of scattering: resonant (R) and nonresonant extreme Klein-Nishina scattering (NR). In reality, the spectrum of ICS photons from an electron of Lorentz factor γ, a subset of which produce pairs, may be produced by scatterings in both the R and NR regimes. However, the first pairs which mark the PFF location will come from one of the two regimes. Thus, in our analytic calculations, to avoid unnecessary complexity, we differentiate between R and NR regimes. Now let us present the expressions for P_* corresponding to these regimes:

For resonant ICS,

$$P_*^{(R)} = 0.1 B_{12}^{6/7} ; \tag{5}$$

and for nonresonant ICS,

$$P_*^{(NR)} = 0.4 B_{12}^{4/7} . \tag{6}$$

In this section we explore the altitudes of PFFs produced by the ICS photons. To estimate the altitude of the PFF above the stellar surface, as in our previous papers (see HM98, eq. [1]; and Paper I, eq. [37]), we can use the expression

$$S_0 = \min[S_a(\gamma_{\min}) + S_p(\varepsilon_{\min})] , \tag{7}$$

where $S_a(\gamma_{\min})$ is the acceleration length that is required for an electron to produce a photon of energy $\varepsilon_{\min}$, and $S_p(\varepsilon_{\min})$ is the photon pair-attenuation length.

For resonant ICS, in the R regime of ICS, the characteristic energy of a scattered photon is

$$\varepsilon \sim 2\gamma B' , \tag{8}$$

where $B' \equiv B/B_{cr}$ (<1) is the local value of the magnetic field strength in units of critical field strength, $B_{cr} = 4.41 \times 10^{13}$ G.

In this paper in our analytic estimates we assume that $B \approx B_0$, which is justified for all cases except for the case of millisecond pulsars. By substituting ε into the expression for S_p (see HM98 or Paper I for details), we get

$$S_p^{(R)} = C_\gamma^{(R)}/\gamma , \tag{9}$$

where $C_\gamma^{(R)} = 2.2 \times 10^{10} P^{1/2}/B_{12}^2$ cm.

As far as the acceleration length S_a is concerned, it is independent of the radiation mechanism (provided that the radiation losses are negligible during acceleration), and the formulae of Paper I (see eqs. [38]) are still applicable. After substituting expressions for S_a and $S_p^{(R)}$ into equation (7), we find that S_0 is minimized at

$$\gamma_{\min}^{(R)} = 10^6 \begin{cases} 0.9 P^{-1/6} B_{12}^{-1} & P \lesssim P_*^{(R)} , \\ 0.2 P^{-3/4} B_{12}^{-1/2} & P \gtrsim P_*^{(R)} . \end{cases} \tag{10}$$

Now we can evaluate equation (7) at $\gamma_{\min}$ to calculate the dimensionless altitude (scaled by a NS radius) of the PFF,

$$z_0^{(R)} \equiv \frac{S_0^{(R)}(\gamma_{\min}^{(R)})}{R} = 10^{-2} \begin{cases} 7 P^{2/3} B_{12}^{-1} & P \lesssim P_*^{(R)} , \\ 17 P^{5/4} B_{12}^{-3/2} & P \gtrsim P_*^{(R)} . \end{cases} \tag{11}$$

For nonresonant ICS, in the NR regime we can use the extreme Klein-Nishina formula, and write for the energy of the scattered photon

$$\varepsilon \sim \gamma . \tag{12}$$

The corresponding photon pair-attenuation length is

$$S_p^{(NR)} = C_\gamma^{(NR)}/\gamma , \tag{13}$$

where $C_\gamma^{(NR)} = 10^9 P^{1/2}/B_{12}$ cm. The expressions for $\gamma_{\min}^{(NR)}$ and $z_0^{(NR)}$ then read

$$\gamma_{\min}^{(NR)} = 10^5 \begin{cases} P^{-1/6} B_{12}^{-1/3} & P \lesssim P_*^{(NR)} , \\ 0.6 P^{-3/4} & P \gtrsim P_*^{(NR)} , \end{cases} \tag{14}$$

and

$$z_0^{(NR)} = 10^{-2} \begin{cases} 3 (P/B_{12})^{2/3} & P \lesssim P_*^{(NR)} , \\ 4 P^{5/4}/B_{12} & P \gtrsim P_*^{(NR)} . \end{cases} \tag{15}$$

The unsaturated regime of equation (14) agrees within a factor of ~ 2 with our numerical calculations for the millisecond and middle-aged pulsars.

2.2.2. Numerical Calculations

The location of the PFF for the different pair-producing radiation processes is more accurately determined using numerical calculations of the minimum height at which the first pairs are produced. Here we incorporate full spatial dependence (in r and θ) of quantities such as the magnetic field and radius of curvature in computing the altitude of the PFF. However, as we discuss in § 3.2, we use a one-dimensional model for the pair dynamics to treat the screening of the electric field about the PFF. The numerical calculation of the altitude of the PFF follows closely that of HM98, but with one notable exception. As discussed above, we use the solutions for $E_\parallel$ with an upper boundary to compute the ICS PFFs (as in HM98) for normal pulsars, whereas we use the solutions for $E_\parallel$ with no upper boundary (but which saturates at infinity) to compute the CR PFFs (as in Paper I) and the ICS PFFs for millisecond pulsars. Otherwise, we have used the same expressions for the energy of pair-producing photons: equation (29) of HM98 for CR photons and equation (43) of HM98 for ICS photons. We have also made the assumption (as in HM98) that the primary electrons travel along the magnetic axis in computing the ICS energy loss and scattering rate. Unlike in the analytic estimates presented, we do not separate the RICS from the NRICS photons, but take a weighted average for the ICS photon energy:

$$\langle \epsilon^{(ICS)} \rangle = \frac{\langle \epsilon^{(R)} \rangle \dot{\gamma}^{(R)} + \langle \epsilon^{(NR)} \rangle \dot{\gamma}^{(NR)}}{\dot{\gamma}^{(R)} + \dot{\gamma}^{(NR)}} . \tag{16}$$

Calculations of z_0 at ICS PFFs as a function of the colatitude ξ for four different sets of pulsar parameters are shown below in Figure 5. Comparison of Figures 5a and 5b confirms that the value of z_0 is independent of PC temperature, since RICS photons have average energies of $2\gamma B'$ and NRICS occurs primarily in the extreme Klein-Nishina limit, where the average scattered photons energy is γ.

With numerical calculation of the PFF altitude, we are able to determine the pulsar parameter space in which the formation of a PFF by the different photon processes is possible [i.e., where $S_p(\epsilon_{\min}) < \infty$]. Figure 1 shows the CR and
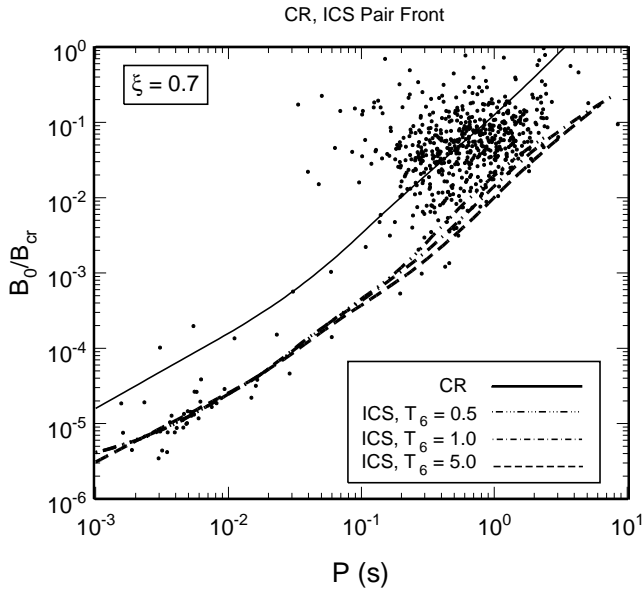
CR, ICS Pair Front

FIG. 1.—Boundaries defining regions in surface magnetic field B_0, in units of critical field, vs. pulsar period, P, where pulsars are capable of producing pairs through curvature radiation (CR) or inverse Compton radiation (ICS). The ICS curves are labeled with different values of PC temperature, T_6, in units of 10^6 K. Also shown are radio pulsars from the ATNF Pulsar Catalog. Pulsars to the right of each line cannot produce pairs by the corresponding process.

ICS PFF parameter space as a function of pulsar period P and surface field strength B_0, as determined by the dipole formula $B_0 = 6.4 \times 10^{19}$ G $(\dot{P}P)^{1/2}$. We have also plotted observed pulsars from the Australia Telescope National Facility (ATNF) catalog,[3] which includes pulsars from the Parkes Multibeam Survey (Manchester et al. 2001) having measured $\dot{P}$. For the B_0 and P values above the lines in Figure 1 for the different processes, we were able to find numerical solutions to equation (7). Pulsars below the lines are therefore not capable of producing pairs from that process. We find that the majority of pulsars cannot produce pairs through CR. This result has been well known for some time (Arons & Scharlemann 1979; Arons 1998; Zhang, Harding, & Muslimov 2000). We find that virtually all known pulsars, with the exception of only a few millisecond pulsars, are capable of producing pairs via ICS. For the majority of pulsars, those with $B_0 \lesssim 0.1 B_{cr}$, the pairs are produced from NRICS photons. We have plotted ICS PFF boundaries for three different temperatures and, as expected, there is only a small dependence on PC temperature. The slight variation due to PC temperature occurs for higher field pulsars where scattering is not in the extreme Klein-Nishina regime and the photon energies become somewhat temperature dependent. The failure of the lowest field millisecond pulsars to produce ICS pairs in our calculation may be due to the failure of our $E_\parallel$ solution, obtained in the small-angle approximation, to accurately model the accelerating field in the millisecond pulsars that have large PCs with $\theta_{pc} \sim 0.3$; or to our use of a canonical NS model in the case of millisecond pulsars that may have undergone significant mass accretion in low-mass binary systems. We are currently exploring these effects to correct this shortcoming. We will also

³ Available at http://www.atnf.csiro.au/pulsar/.

examine the possibility of photon-photon pair formation in millisecond pulsars. We discuss the broader implication of pair death lines in § 4.

3. RETURNING POSITRON FRACTION AND ELECTRIC FIELD SCREENING BY PAIRS

3.1. *Analytic Estimates*

To estimate the maximum fractional density of positrons returning from the upper PFFs we can use equation (33) of Paper I and the expressions for z_0 derived in § 2.2. We must note, however, that in Paper I (where we investigated the CR case alone) in our analytic calculations of the fraction of returning positrons, we justifiably assumed that the screening occurs within the length scale much less than z_0. This is not the case for ICS, for which the screening scale is determined by the scale of growth of energy of pair-producing photons. For the ICS photons the energy of pair-producing photons $\sim \gamma$, so that the scale of growth of γ governs the screening scale Δ_s, i.e.,

$$\Delta_s \sim \left[\frac{\gamma}{d\gamma/dz}\right]_{z=z_0} \approx \begin{cases} 0.5z_0 & P \lesssim P_*^{(R,NR)} , \\ z_0 & P \gtrsim P_*^{(R,NR)} . \end{cases} \quad (17)$$

Thus, in the case of ICS the screening effectively occurs over a more extended region. This means that even within the screening region the primary electrons keep accelerating and generating pair-producing photons. Since the pair-production rate per primary electron in the case of the ICS photons is not as high as in the case of CR photons, the assumption that the altitude of the screening is z_0 would result in a significant underestimation of the returning positron fraction at the ICS-controlled pair fronts. To come up with better estimates we should add Δ_s to the calculated values of z_0, or, according to equation (17), multiply z_0 by a factor of 1.5 and 2 for the unsaturated and saturated regimes, respectively.

Evaluating expressions for ρ_+/ρ_{GJ} (where ρ_+ is the charge density of returning positrons, and ρ_{GJ} is the Goldreich-Julian charge density; see also eq. [33] of Paper I) at $z_* = z_0 + \Delta_s$, we get for resonant ICS,

$$\left(\frac{\rho_+}{\rho_{GJ}}\right)^{(R)} = 10^{-2} \begin{cases} 2P^{2/3}/B_{12} & P \lesssim P_*^{(R)} , \\ 5P^{5/4}/B_{12}^{3/2} & P \gtrsim P_*^{(R)} , \end{cases} \quad (18)$$

and for nonresonant ICS,

$$\left(\frac{\rho_+}{\rho_{GJ}}\right)^{(NR)} = 10^{-3} \begin{cases} 7(P/B_{12})^{2/3} & P \lesssim P_*^{(NR)} , \\ 9(P^{5/4}/B_{12}) & P \gtrsim P_*^{(NR)} . \end{cases} \quad (19)$$

In their paper HA01 assume that the fraction of returning positrons (see § 5.3) is of the order of $\kappa r_{pc}/R$, where $r_{pc} (\approx 10^4/P^{1/2}$ cm) is the PC radius, and R is the NS radius $(=10^6$ cm). In contrast, in our calculations the fractional density of returning positrons is proportional to the dimensionless screening altitude (see Paper I), and can be roughly estimated as $1.5[\kappa/(1-\kappa)]z_0$. Thus, the ratio of our value for the density of returning positrons to that of HA01 is of the order of S_0/r_{pc}, which for the observed pulsar parameters may range from ~ 0.1 to ~ 20. More specifically, for short-period pulsars our calculated fractions of returning positrons are up to a factor of ~ 10 less than those of HA01, while for relatively long period pulsars they are larger by

about the same factor. Besides this quantitative difference, there is a significant difference in the dependence of our fractional densities on B and P. Note that in reality, the screening scale and thus also ρ_+/ρ_{GJ} depend on the PC temperature, as will be shown in the numerical calculations. We cannot model this dependence analytically, since we have assumed that the Δ_s is a constant multiple of z_0 for all pulsars.

3.2. Numerical Calculations

Our numerical calculation of the returning positron fraction and scale length of the ICS pair screening follows that described in Paper I for CR pair screening. As detailed in that paper, we first compute the pair source function in energy and altitude above the PFF and then compute the dynamical response of the pairs to the $E_\parallel$ above the PFF by solving the continuity and energy equations of the pairs to obtain the charge density. The $E_\parallel$ above the PFF is parameterized as an exponential with scale height Δ_s, which is readjusted at each iteration to equal a multiple of the height at which the computed charge density from the pairs equals the difference between the primary beam charge density and Goldreich-Julian charge density. In computing the source function of pairs from ICS photons, we consider a hybrid spectrum of RICS and NRICS photons from the primary particle, of Lorentz factor γ, at a given altitude of its acceleration. In the ICS photon spectrum, photons with energies $\epsilon < 2\gamma B'$ are produced primarily by RICS. Since the RICS spectrum from a single electron cuts off sharply for photon energies $\epsilon \simeq 2\gamma B'$, photons above this energy, up to a maximum energy of $\epsilon = \gamma$, will be produced by NRICS. We therefore describe the ICS photon spectrum for $\epsilon < 2\gamma B'$ by a RICS spectrum based on an expression given by Dermer (1990). Assuming delta function distributions of electrons of Lorentz factor γ, and thermal photons of energy $\epsilon_0 = 2.7 kT/mc^2$ and incident angles $\mu_- < \mu < \mu_+$ in the laboratory frame, Dermer's (1990) equation (10) for the distribution of scattered photons with energy ϵ_s, integrated over scattered angles $-1 < \mu_s < 1$, becomes

$$\frac{N^R(\epsilon_s)}{dt\, d\epsilon_s} = \frac{c\sigma_T \epsilon_B}{2(\mu_+ - \mu_-)} \frac{1}{\beta^2\gamma^3} \frac{n_0}{\epsilon_0^2}\left[J_0 + J_1 + \frac{1}{2}(J_2 - J_1)\right], \quad (20)$$

where $J_n = I_n(\mu_+) - I_n(\mu_-)$,

$$u_+ = \gamma\epsilon_B^{-1}\max[\epsilon_s/2\gamma^2,\ \epsilon_0(1 - \beta\mu_+)],$$
$$u_- = \gamma\epsilon_B^{-1}\min[2\epsilon_s,\ \epsilon_0(1 - \beta\mu_-)], \quad (21)$$

and

$$I_0(u) = \frac{3}{(4\beta\gamma\epsilon_B)^4}\left[\frac{-\epsilon_0^2\epsilon_s^2}{3u^3} + \frac{\gamma\epsilon_0\epsilon_s\epsilon_B(\epsilon_0 + \epsilon_s)}{u^2}\right.$$
$$\left. - \frac{\epsilon_B(\epsilon_0^2 + \epsilon_s^2 + 4\gamma^2\epsilon_0\epsilon_s)}{u} - 2\gamma\epsilon_B^2(\epsilon_0 + \epsilon_s)\ln u + \epsilon_B^4 u\right], \quad (22)$$

$$I_1(u) = u - (u+1)^{-1} - 2\ln(u+1), \quad (23)$$

$$I_2(u) = u + \ln[(u-1)^2 + a^2] + (a^{-1} + a)\tan^{-1}\left[\frac{(u-1)}{a}\right], \quad (24)$$

where σ_T is the Thompson cross section, β is the electron velocity in units of the velocity of light, $\epsilon_B = B/B_{cr}$ is the cyclotron energy in units of mc^2, $a = 2\alpha_f\epsilon_B/3$, α_f is the fine-structure constant, and $n_0 = 20\ \mathrm{cm}^{-3}\ T^3$ is the density of thermal photons of energy ϵ_0. Each scattered photon is assumed to be emitted along the direction of the particle momentum (i.e., along the local magnetic field). Although the distribution of scattered photon angles depends on energy (see Fig. 3 of Dermer 1990), the photons at pair-producing energies scattered by relativistic electrons are mostly emitted along the field direction. Since we will be treating scattering of both upward-moving electrons and downward-moving positrons, we have

$$\text{for electrons}: \quad \mu_- = \mu_c, \quad \mu_+ = 1; \quad (25)$$
$$\text{for positrons}: \quad \mu_- = -1, \quad \mu_+ = -\mu_c \quad (26)$$

in equation (21), where

$$\mu_c = \cos\theta_c = \frac{h}{\sqrt{h^2 + r_t^2}} \quad (27)$$

is the largest scattering angle at height h above the NS surface, and $r_t = r_{pc} \ll R$ is the radius of the hot PC.

The ICS photon spectrum for $\epsilon > 2\gamma B'$ is produced by NRICS. We use a spectrum for relativistic (but nonmagnetic) scattering that is based on an expression of Jones (1968), derived originally to apply to scattering of an isotropic distribution of photons by a relativistic electron, which we have modified to apply to a semi-isotropic distribution of thermal photons,

$$\frac{N^{NR}(\epsilon_s)}{dt\, d\epsilon_s} = \frac{n_0\pi r_0^2 c\lambda_\pm}{\gamma^2\epsilon_0}$$
$$\times \left[2q\ln q + (1 + 2q)(1 - q)\right.$$
$$\left. + \frac{(q\Gamma_0)^2}{(1 + q\Gamma_0)}\frac{(1 - q)}{2}\right], \quad (28)$$

where

$$q = \frac{E_s}{\Gamma_0(1 - E_s)}, \quad E_s = \frac{\epsilon_s}{\gamma}, \quad \Gamma_0 = 2\gamma\epsilon_0\lambda_\pm. \quad (29)$$

Here r_0 is the classical electron radius. For upward-moving electrons $\lambda_- = (1 - \beta\mu_c)$, and for downward-moving positrons $\lambda_+ = 2$.

Our method for calculating the pair source function from ICS photons is similar to that used in Paper I for CR photons. However, unlike in the case of CR, higher generations of pairs from synchrotron radiation of first-generation pairs are important in the screening, since the attenuation length for the synchrotron photons is less than the ICS screening scale. As in Paper I, the contribution to the pair source function from first-generation pairs is computed by dividing the ICS spectrum radiated by the primary particle at each step along its path into discrete energy intervals. A representative photon from each ICS energy bin is propagated through the local field to determine whether it escapes or produces a pair, in which case the location of the pair is recorded (for details of such a calculation, see Paper I and Harding, Baring, & Gonthier 1997). The pairs for each ICS spectral energy interval of width $\Delta\epsilon_s$ are then weighted in the source function by the "number" of RICS or NRICS

photons, $n^{\mathrm{R,NR}}$, represented by the test photon in that energy bin, estimated by integrating the photon spectrum over the bin

$$n^{\mathrm{R,NR}}(\epsilon_s) = \frac{\Delta s}{c} \int_{\epsilon_s - \Delta \epsilon_s/2}^{\epsilon_s + \Delta \epsilon_s/2} \frac{N^{\mathrm{R,NR}}(\epsilon_s')}{dt\, d\epsilon_s'}\, d\epsilon_s' , \qquad (30)$$

where Δs is the size of the particle path length.

The contribution of higher generations of pairs to the source spectrum is computed by simulating a pair cascade in the method described by Baring & Harding (2001), except that we do not include the possibility of photon splitting in the present calculation. By limiting the surface magnetic field we consider to $B_0 < B_{\mathrm{cr}}$, we can safely neglect splitting. As described in Baring & Harding (2001), the created pairs from the first generation make transitions between Landau states to radiate synchrotron/cyclotron photons until they reach the ground Landau state. Each synchrotron/cyclotron photon is individually traced through the local magnetic field until it either escapes or creates a pair, which radiates another generation of photons. A recursive routine is called upon the radiation of each photon, so that a large number of pair generations can be simulated.

One notable difference was introduced in the present cascade simulation in order to treat the synchrotron radiation from millisecond pulsars. The low surface fields of the millisecond pulsars, combined with the photon energies $\epsilon \sim 10^6$–10^7 required to produce pairs, give very large Landau states for the created pairs, making it impossible to treat the synchrotron/cyclotron photon emission discretely. For local fields $B < 0.01 B_{\mathrm{cr}}$, we treated the synchrotron radiation from the pairs by the same method as for the ICS radiation from the primaries, i.e., as a continuous spectrum. To describe the total spectrum radiated by a particle as it decays from a high initial Landau state (i.e., large initial pitch angle) to the ground state (zero pitch angle), we use the calculated synchrotron spectrum of Tademaru (1973),

$$N_s(\epsilon)d\epsilon = \frac{1}{2}(B' \sin \psi_0)^{-1/2} \epsilon^{-3/2} d\epsilon , \qquad (31)$$

where ψ_0 is the initial pitch angle of the particle and $B' = B/B_{\mathrm{cr}}$ is the local magnetic field strength. Surprisingly, for the millisecond pulsars we are required to limit the upper end of the synchrotron spectrum at an energy equal to the particle Lorentz factor in order to avoid violating energy conservation. This is a well-known problem in high magnetic fields (e.g., Harding & Preece 1987), but in this case the very high Lorentz factors of the pairs give a synchrotron critical energy $\epsilon_{\mathrm{cr}} = (3/2)\gamma^2 B' \sin \psi_0 > \gamma$. Imposing the energy-conservation condition limits the number of pair generations. The discrete QED treatment of the synchrotron emission in high magnetic fields (described above) is able to treat the effect of pair production in the ground Landau state, which also severely limits the number of pair generations in fields $B \gtrsim 0.2 B_{\mathrm{cr}}$ (Baring & Harding 2001).

3.2.1. *Screening Effect at the Upper Pair Front*

Since the ICS photon spectrum has a much weaker dependence on the particle Lorentz factor than the CR photon spectrum, the ICS pair source function grows much more slowly with height above the PFF. In the case of NRICS, the photon emission rate decreases as $\sim 1/\gamma$, while the RICS emission rate first increases sharply at low γ as the soft photons come into resonance in the particle rest frame,

and then decreases as $1/\gamma^2$, whereas in the case of CR the photon emission rate increases as γ. Even though the characteristic ICS photon energies are increasing with γ, the stronger decrease in photon number with height as the particle accelerates, combined with the decrease in soft photon density and angle with altitude, makes screening by pairs produced by ICS photons much more difficult and in some cases impossible. In nearly all cases, the screening scale lengths are comparable to the particle acceleration length, requiring different treatment of the self-consistent screening calculation from what was used in Paper I for CR screening. The onset of pair production and possible screening close to the NS surface couples the entire $E_\parallel$ solution to the screening scale. We therefore must correct the accelerating $E_\parallel$ as well as the $E_\parallel$ in the screening region above the PFF on every iteration of the screening scale length. This is done by adjusting the upper boundary of the $E_\parallel$ solution (eqs. [A7]–[A10] of Paper I) to $z_0 + \Delta_s$, so that the electric potential distribution below the pair front is accurate. We still assume the exponential form with scale height Δ_s (eq. [26] of Paper I) for $E_\parallel$ above the PFF. But unlike our calculation of CR pair screening, the location of the PFF will change and adjust on every iteration of Δ_s. The exponential function $E_\parallel^{\mathrm{sc}}(z \gtrsim z_0) = E_\parallel^{\mathrm{acc}}(z_0) \exp[-(z - z_0)/\Delta_s]$ describing the $E_\parallel$ above the PFF is also renormalized at the PFF at each iteration so that the value of $E_\parallel^{\mathrm{acc}}(z_0)$ is equal to the maximum value of the $E_\parallel$ solution between $z = 0$ and $z = z_0 + \Delta_s$. We also must take into account the increase in the charge deficit in the screening region, which will also cause ICS screening to be more difficult.

Figure 2 shows an example of an ICS pair source function, integrated over energy, so that the growth of pairs as a function of distance $x = z - z_0$ above the PFF is displayed. The first generation of pairs (those produced by primary electrons) is almost flat before beginning to decrease. Including pairs from higher cascade generations produces an initially sharp increase in number of pairs versus height, but the pair number quickly levels off and also eventually decreases. The ICS pair source function is a sharp contrast to the CR pair source function shown in Figure 1 of Paper I,
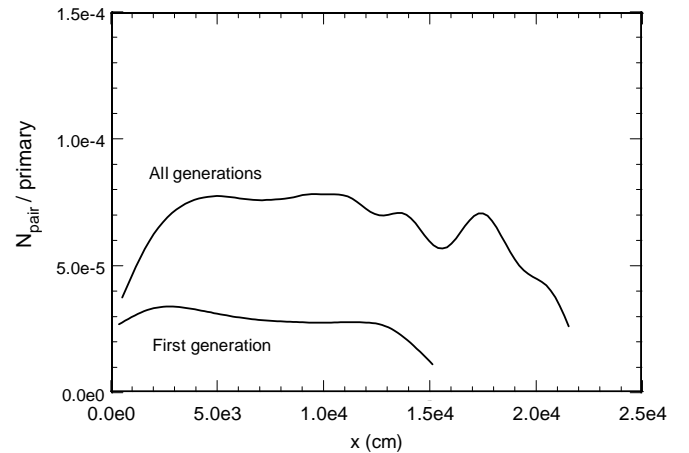

FIG. 2.—Example of electron-positron pair source function integrated over energy, as a function of distance, x, above the pair-formation front produced by a pair cascade initiated by inverse Compton radiation from primary electrons. The vertical axis measures the number of pairs produced in each spatial bin, normalized per primary electron. Both curves are for $P = 0.1$ s, $B/B_{\mathrm{cr}} = 0.1$, $T_6 = 0.5$, and colatitude $\xi = 0.7$, in units of PC half-angle.
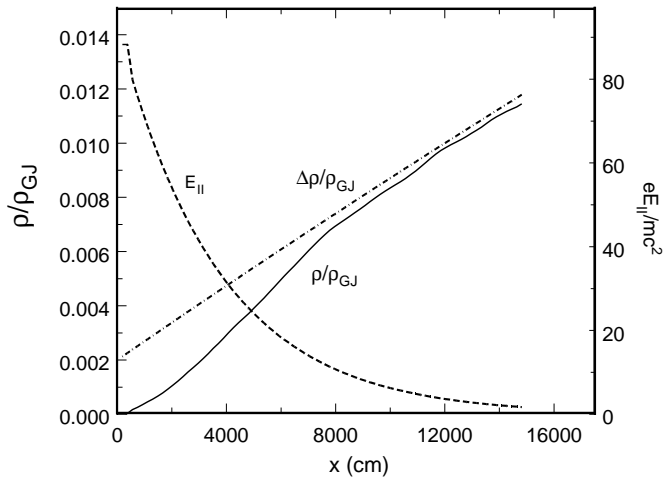
Fig. 3.—Self-consistent solution for the charge density, $\rho(x)$, due to trapped positrons, which asymptotically approaches the charge deficit, $\Delta\rho$, needed to screen the electric field, $E_\parallel$, above the PFF, modeled as a declining exponential with screening scale height, $\Delta_s R$; x is the distance above the pair front. The pulsar parameters are the same as those of Fig. 2, except that $T_6 = 1$ here.
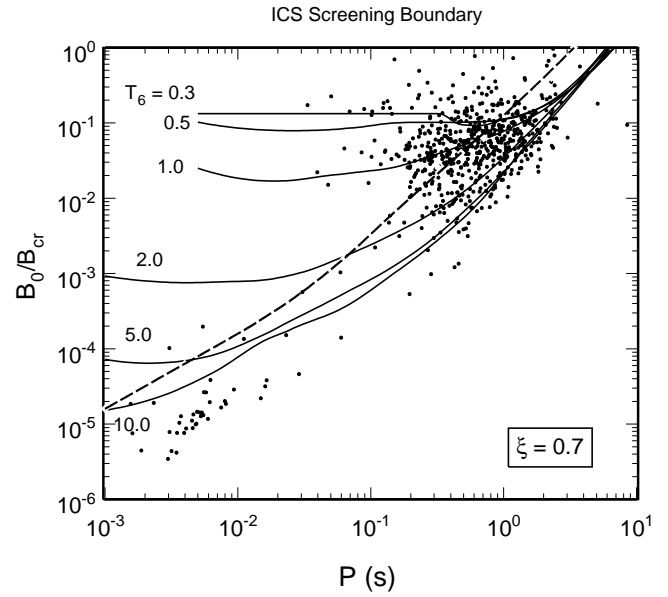

Fig. 4.—Boundaries in surface magnetic field B_0 (in units of critical field) vs. pulsar period, P, above which locally complete screening of $E_\parallel$ occurs above the ICS pair front. Curves are labeled with values of the PC temperature T_6, in units of 10^6 K. The dashed curve is the CR pair boundary (as shown in Fig. 1).

which increases nearly exponentially with height above the PFF. This raises the interesting question of whether ICS pairs are capable of screening $E_\parallel$ to all altitudes, even if they are able to initially screen the local $E_\parallel$. Figure 3 shows an example of a self-consistent solution for the charge density $\rho(x)/\rho_{GJ}$ due to polarization of pairs and Δ_s in the screening region. The charge density initially increases faster than the charge deficit, which is increasing approximately as x. In this case, screening of $E_\parallel$ is achieved locally, until the pair source function begins to decline with x, causing the charge density due to pairs to decrease. As the charge density due to pairs decreases while the charge deficit is increasing, screening cannot be maintained and the $E_\parallel$ will again begin to grow. We cannot model this effect in the present calculation, which would require the solution of Poisson's equation throughout the screening region. However, it is clear that ICS screening cannot short-out $E_\parallel$ and produce a limit to particle acceleration at low altitudes. ICS screening, even if locally complete, will only slow the particle acceleration until the ICS pair density falls off, and beyond this point the particles will resume their acceleration until they can produce CR pairs, which will then screen the $E_\parallel$ at higher altitudes.

For many pulsars, however, ICS cannot even achieve locally complete screening. Figure 4 shows computed boundaries of ICS local screening for different assumed PC temperatures, $T_6 \equiv T/10^6$ K, as a function of pulsar surface magnetic field and period. Pulsars above and to the left of these boundaries can achieve local screening of $E_\parallel$ at a colatitude of $\xi = 0.7$, while pulsars below and to the right of the boundaries cannot. Although the PFF boundaries were nearly independent of T_6, the screening boundaries are very sensitive to the temperature of the soft photons. For low T_6, only very high field pulsars, those whose pairs source functions are dominated by RICS, can screen with ICS photons. As T_6 increases, the boundaries move down, but are limited in their movement to the right as they approach the ICS PFF boundaries (Fig. 1). There is also some dependence of the screening boundaries on ξ, in that the boundary for a given T_6 will be higher at a lower value of ξ. This means that

screening is more difficult in the inner parts of the PC, so that some pulsars may have local ICS screening only in the outer part of their PC.

Even though complete ICS screening is not achieved for all pulsars, there will still be positrons that turn around and return to heat the PC. In fact this heating can be substantial, since in the absence of complete screening that shuts off the acceleration, most of the positrons from ICS pairs will return to the PC. Figure 5 shows self-consistent calculations of the returning positron fraction, as well as the PFF altitude z_0, which we have discussed in § 2.2, as a function of ξ. Figures 5a and 5b, which have the same P and B values but temperatures $T_6 = 0.5$ and 3.0, respectively, illustrate that although there is very little difference in the PFF altitude with a large increase in PC temperature, there is a large increase in returning positron fraction. The dependence of ρ^+/ρ_{GJ} on T_6 is not reflected in the analytic estimates (eqs. [18] and [19]), which are based only on a constant multiple of the charge deficit at the PFF altitude, proportional only to z_0. The size of ρ^+/ρ_{GJ} is actually dependent on the number of pairs produced above z_0, which is not dependent on the charge deficit if screening is not achieved. Comparison of Figures 5a and 5c shows that pulsars with larger periods have relatively larger z_0 and also larger fractions of returning positrons. This is due to the fact that longer period pulsars have more difficulty producing pairs because of the smaller PC size and therefore larger radii of curvature of the last open field line. As illustrated in Figure 5d, millisecond pulsars have very large z_0 and large fractions of returning positrons, but smaller than expected from the analytic solutions, because they do not produce enough pairs to screen the field.

Figure 6 shows the dependence of returning positron fraction on PC temperature T_6 and surface field strength. The steep dependence of ρ^+/ρ_{GJ} on T_6 at low temperatures $T_6 < 1.0$ is due to the increase in numbers of high-energy ICS photons that produce pairs. For $T_6 > 1.0$, in the case of
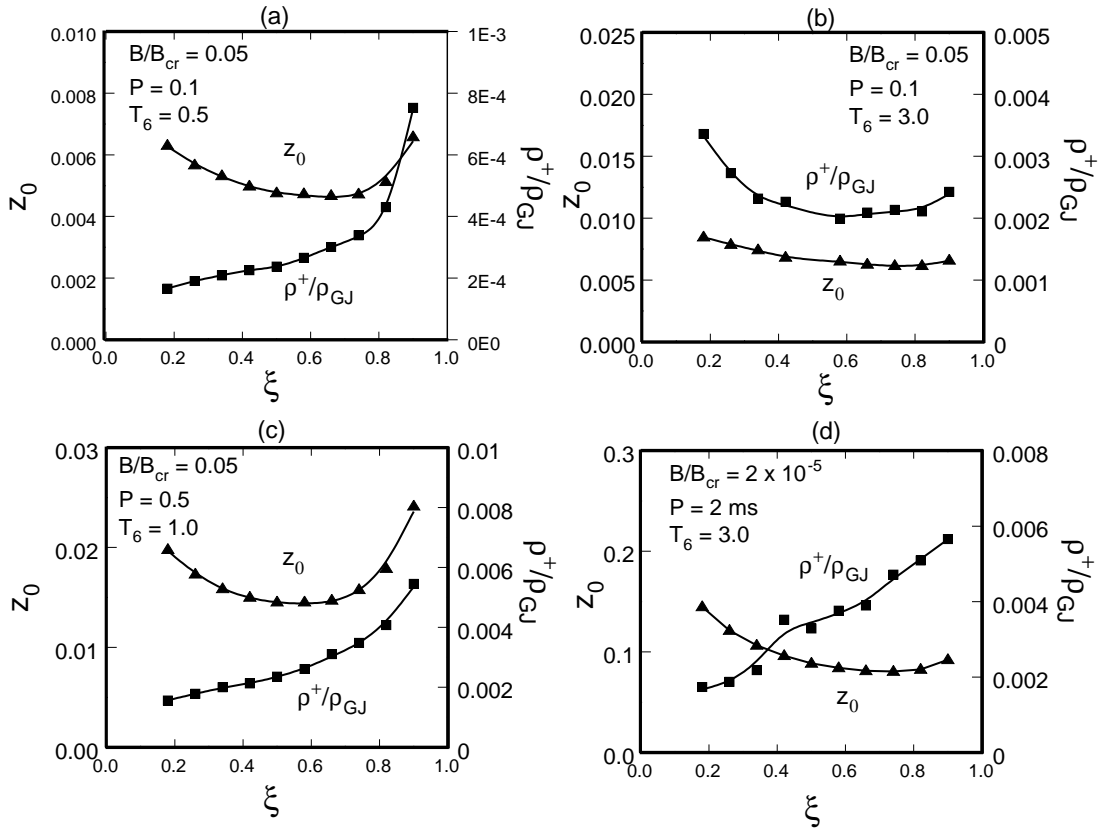
FIG. 5.—Solutions for the returning (trapped) positron density, ρ^+/ρ_{GJ}, normalized to the Goldreich Julian density and pair-formation front altitude, z_0, in units of NS radius, as a function of magnetic colatitude, ξ, which has been normalized to the PC half-angle.

normal pulsars there is local screening at these field strengths, which limits the number of returning positrons to be proportional to $(z_0 + \Delta_s)$ rather than to T_6. The screening therefore produces a saturation in the PC heating, which will be seen in the calculation of PC heating luminosities presented in § 5.

3.2.2. *Screening at Lower Pair Fronts*

As discussed in HM98, the positrons returning from the upper PFF will be accelerated through the same voltage drop as the primary electrons and thus will reach the same high energies as the primaries that produced them. They will therefore initiate pair cascades as they approach the NS surface. HM98 speculated that the pairs from these downward-moving cascades may screen the $E_\parallel$ above the surface, since they found that the PFFs of the positrons are located at significant altitudes above the surface, due to asymmetry in the ICS between upward-moving and downward-moving particles. Now that we can calculate the fraction of positrons returning from the upper ICS PFF, we can investigate the question of screening at the lower PFF. We have simulated cascades below the PFFs of test positrons returning from the upper PFF. The source functions of pairs from the downward cascades and the charge density are computed in the same way as at the upper PFF, and the screening scale height is determined self-consistently. But there are several critical differences between screening at upper and lower PFFs. First, the flux of returning positrons from the ICS PFF is small compared to the primary flux, and the charge density must be weighted with the value ρ^+/ρ_{GJ}. Second,

the value of $E_\parallel$ is very small near the NS surface, making it harder to turn around the electrons from the pairs. Third, the charge deficit is much smaller than at the upper PFF and decreasing toward the stellar surface, being proportional to
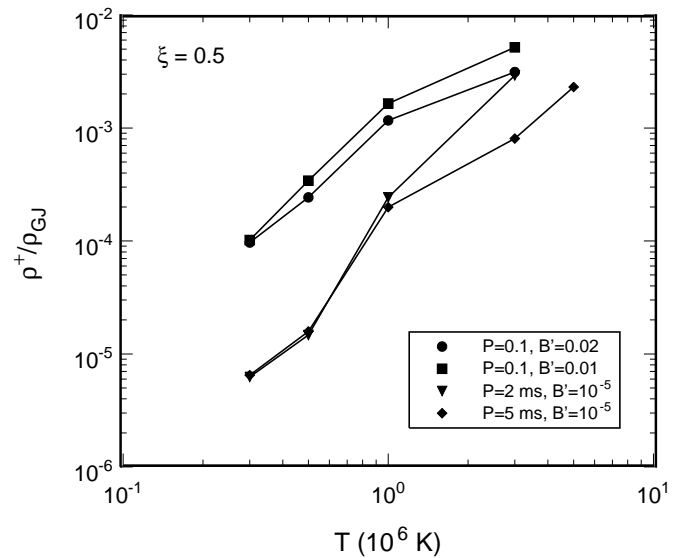

FIG. 6.—Solutions for the returning (trapped) positron density, ρ^+/ρ_{GJ}, normalized to the Goldreich Julian density as a function of PC temperature T_6, in units of 10^6 K, for different values of surface magnetic field strength in units of the critical field, B/B_{cr}.

the altitude of the returning positron pair front. This guarantees that there will be a point above the NS surface where $\rho(x)/\rho_{GJ}$ will equal the charge deficit.

We have computed pair source functions from cascades of downward-moving positrons and the resulting charge densities below the lower PFF for a range of pulsar parameters. We find that for nearly all pulsars, the charge densities do not reach values high enough to screen $E_\parallel$ significantly above the NS surface. For pulsars having surface fields $B \lesssim 0.1B_{cr}$ and periods $P < 0.5$, pair multiplicities from the near-surface cascades are not high enough to balance the low fraction of returning positrons, primarily because most pairs are produced in the ground Landau state in the high near-surface fields. For pulsars having lower surface fields and longer periods, screening can occur for some cases just above the surface at the highest PC temperatures. These pulsars are near the ICS screening boundary (Fig. 4). Therefore, according to our calculations it seems that ICS PFFs will be stable except possibly near the screening boundaries.

4. ENERGETICS OF PRIMARY BEAM AND PULSAR DEATH LINE

4.1. *Luminosity of Primary Beam*

Before we discuss the pulsar death line, it is instructive to calculate the luminosity of the primary electron beam at the PFF.

The luminosity of the primary beam as a function of z ($\ll 1$) can be written as (see eq. [73] of MH97, and cf. eq. [61] of Paper I)

$$L_{prim} = \alpha c \int_{S(z)} \rho(z,\xi) \Phi(z,\xi) \, dS , \qquad (32)$$

where $\alpha = (1 - r_g/R)^{1/2}$ (r_g is the gravitational radius of a NS of radius R), ρ is the charge density of the electron beam, Φ is the electrostatic potential, $dS = r_{pc}^2 \, d\Omega_\xi$, and $d\Omega_\xi = \xi \, d\xi \, d\phi$ is an element of solid angle in the PC region (see also Paper I for details). Here the integration is over the area of a sphere cut by the polar flux tube at altitude z.

Similar to our derivation of equations (63)–(65) of Paper I, we can write for the luminosity of the primary beam

$$L_{prim} = f_{prim} \dot{E}_{rot} , \qquad (33)$$

where $\dot{E}_{rot}$ is the pulsar spin-down luminosity [$= \Omega^4 B_0^2 R^6 / 6c^3 f^2(1)$, where $B_0/f(1)$ is the surface value of the magnetic field strength corrected for the general-relativistic redshift; see eq. [66] of Paper I for details], and f_{prim} is the efficiency of converting spin-down luminosity into the luminosity of the primary beam. Thus, by comparing the above two equations, we can get the following expression for f_{prim}:

$$f_{prim} = 6 \times 10^{-3} P^{-1/2} \zeta \begin{cases} \zeta & P \lesssim P_*^{(CR,R,NR)} , \\ 0.6 & P \gtrsim P_*^{(CR,R,NR)} , \end{cases} \qquad (34)$$

where ζ is the altitude scaled by the PC radius, r_{pc}. In the derivation of equation (34), we assumed $\kappa = 0.15$ and $\cos\chi \approx 1$.

Now we should evaluate equation (34) at the altitude beyond the PFF where the electric field is screened, or at

$\zeta_* = \zeta_0 + \Delta_s R/r_{pc}$. For the CR case $\zeta_* \approx \zeta_0$, while for the ICS pair fronts (for both R and NR regimes; see also eq. [17])

$$\zeta_* \approx \begin{cases} 1.5\zeta_0 & P \lesssim P_*^{(R,NR)} , \\ 2\zeta_0 & P \gtrsim P_*^{(R,NR)} . \end{cases} \qquad (35)$$

After substituting ζ_0 we get the following explicit expressions for ζ_*:

For curvature radiation,

$$\zeta_*^{(CR)} = \begin{cases} 30(P^{9/7}/B_{12}^{4/7}) = 2B_{12}^{5/7}\tau_6^{9/14} & P \lesssim P_*^{(CR)} , \\ 430(P^{9/4}/B_{12}) = 4B_{12}^{5/4}\tau_6^{9/8} & P \gtrsim P_*^{(CR)} ; \end{cases} \qquad (36)$$

for resonant ICS,

$$\zeta_*^{(R)} = \begin{cases} 10(P^{7/6}/B_{12}) = B_{12}^{1/6}\tau_6^{7/12} & P \lesssim P_*^{(R)} , \\ 30(P^{7/4}/B_{12}^{3/2}) = B_{12}^{1/4}\tau_6^{7/8} & P \gtrsim P_*^{(R)} ; \end{cases} \qquad (37)$$

and for nonresonant ICS,

$$\zeta_*^{(NR)} = \begin{cases} 3(P^{7/6}/B_{12}^{2/3}) = 0.3B_{12}^{1/2}\tau_6^{7/12} & P \lesssim P_*^{(NR)} , \\ 6(P^{7/4}/B_{12}) = 0.2B_{12}^{3/4}\tau_6^{7/8} & P \gtrsim P_*^{(NR)} , \end{cases} \qquad (38)$$

where $\tau_6 = \tau/10^6$ yr $= 65(P/B_{12})^2$. Inserting equations (36)–(38) into equations (33) and (34), we get for curvature radiation,

$$L_{prim}^{(CR)} = 10^{32} \text{ ergs s}^{-1}$$
$$\times \begin{cases} 0.3(P^{-27/14}B_{12}^{6/7}) = 20B_{12}^{-15/14}\tau_6^{-27/28} & P \lesssim P_*^{(CR)} , \\ 0.1(P^{-9/4}B_{12}) = 10B_{12}^{-5/4}\tau_6^{-9/8} & P \gtrsim P_*^{(CR)} , \end{cases} \qquad (39)$$

or

$$L_{prim}^{(CR)} = 10^{16} \text{ (ergs s}^{-1})^{1/2} \dot{E}_{rot}^{1/2}$$
$$\times \begin{cases} P^{1/14}B_{12}^{-1/7} & P \lesssim P_*^{(CR)} , \\ 0.3P^{-1/4} & P \gtrsim P_*^{(CR)} , \end{cases} \qquad (40)$$

$$f_{prim}^{(CR)} = 0.01 \begin{cases} 7(B_{12}^{13/14}\tau_6^{29/28}) & P \lesssim P_*^{(CR)} , \\ 5(B_{12}^{3/4}\tau_6^{7/8}) & P \gtrsim P_*^{(CR)} ; \end{cases} \qquad (41)$$

for resonant ICS,

$$L_{prim}^{(R)} = 10^{31} \text{ ergs s}^{-1}$$
$$\times \begin{cases} 0.3P^{-13/6} = 30(B_{12}^{-13/6}\tau_6^{-13/12}) & P \lesssim P_*^{(R)} , \\ 0.05(P^{-11/4}B_{12}^{1/2}) = 20(B_{12}^{-9/4}\tau_6^{-11/8}) & P \gtrsim P_*^{(R)} , \end{cases} \qquad (42)$$

or

$$L_{prim}^{(R)} = 10^{15}(\text{ergs s}^{-1})^{1/2} \dot{E}_{rot}^{1/2}$$
$$\times \begin{cases} P^{-1/6}B_{12}^{-1} & P \lesssim P_*^{(R)} , \\ 0.2(P^{-3/4}B_{12}^{-1/2}) & P \gtrsim P_*^{(R)} , \end{cases} \qquad (43)$$

$$f_{\text{prim}}^{(R)} = 10^{-2} \begin{cases} B_{12}^{-1/6}\tau_6^{11/12} & P \lesssim P_*^{(R)} , \\ 0.8(B_{12}^{-1/4}\tau_6^{5/8}) & P \gtrsim P_*^{(R)} ; \end{cases} \quad (44)$$

and for nonresonant ICS,

$$L_{\text{prim}}^{(NR)} = 10^{30} \text{ ergs s}^{-1}$$
$$\times \begin{cases} 0.3(B_{12}^{2/3}P^{-13/6}) = 30(B_{12}^{-3/2}\tau_6^{-13/12}) & P \lesssim P_*^{(NR)} , \\ 0.1(B_{12}P^{-11/4}) = 30(B_{12}^{-7/4}\tau_6^{-11/8}) & P \gtrsim P_*^{(NR)} , \end{cases}$$
$$(45)$$

or

$$L_{\text{prim}}^{(NR)} = 10^{15}(\text{ergs s}^{-1})^{1/2}\dot{E}_{\text{rot}}^{1/2}$$
$$\times \begin{cases} 0.1(B_{12}^{-1/3}P^{-1/6}) & P \lesssim P_*^{(NR)} , \\ 0.05P^{-3/4} & P \gtrsim P_*^{(NR)} , \end{cases} \quad (46)$$

$$f_{\text{prim}}^{(NR)} = 10^{-3} \begin{cases} B_{12}^{1/2}\tau_6^{11/12} & P \lesssim P_*^{(NR)} , \\ 2(B_{12}^{1/4}\tau_6^{5/8}) & P \gtrsim P_*^{(NR)} . \end{cases} \quad (47)$$

The above formulae are just different representations of the luminosity that a primary (electron) beam achieves by the moment the $E_\parallel$ is screened, for each of the radiation processes we discuss. Note that the eight known EGRET γ-ray pulsars fit an empirical relation $L_\gamma \propto \dot{E}_{\text{rot}}^{1/2}$. This is reproduced by the above expression for the luminosity of the primary beam at the CR PFF if the primary electrons are nearly 100% efficient at conversion of their energy to high-energy γ-rays (see Zhang & Harding 2000), but not by the luminosity at the ICS pair fronts. But we have argued that the primary particle acceleration is not stopped at the ICS PFF, so that the potential drop at the CR PFF determines the final acceleration energy and thus the γ-ray luminosity of the pulsar.

4.2. Derivation of Theoretical Pulsar Death Line

4.2.1. Analytic Approach

In pulsar physics the term "death line" was originally introduced for radio pulsars and refers to a line separating the domain (normally in the P-$\dot{P}$ diagram) favoring pair formation from the domain where pair formation does not occur. Most PC models for radio pulsars imply therefore that radio emission turns off (see Sturrock 1971; Ruderman & Sutherland 1975; Chen & Ruderman 1993) if the potential drop required for pair production exceeds the maximum that can be achieved over the PC. This concept of death line implicitly assumes that the pair formation is a necessary condition for pulsar radio emission, and that pulsars become radio quiet after crossing the death lines during their evolution. Some authors argue that this condition may not be sufficient, however. For example, HA01 define a pulsar's death as the condition when pair production is too weak to generate the pair cascade multiplicity required to screen the accelerating electric field. We believe that pair formation is vital for pulsar operation, but we suggest that the pairs required for radio emission may not necessarily screen or shut off the accelerating electric field (see also Paper I). In addition, we adopt a canonical definition of a pulsar's death as an essentially pairless regime of operation.

In general, to write a formal criterion specifying the death line one needs to know the characteristic voltage drop in the pulsar acceleration region. For the acceleration model we employ in our study this voltage drop can be calculated as

$$\Delta\Phi_{\text{acc}} = 10^{10} \text{ V } B_{12}P^{-5/2}\zeta \begin{cases} 3\zeta & P \lesssim P_*^{(CR,R,NR)} , \\ 2 & P \gtrsim P_*^{(CR,R,NR)} . \end{cases} \quad (48)$$

The corresponding calculated Lorentz factor of a primary electron accelerating from the PC is

$$\gamma_{\text{acc}} = \frac{e}{mc^2}\Delta\Phi_{\text{acc}}$$
$$= 10^4 B_{12}P^{-5/2}\zeta \begin{cases} 6\zeta & P \lesssim P_*^{(CR,R,NR)} , \\ 4 & P \gtrsim P_*^{(CR,R,NR)} . \end{cases} \quad (49)$$

Thus, our criterion for the pulsar death line separating radio-active from radio-quiet pulsars translates into

$$\gamma_{\text{acc}} \geq \gamma_{\text{min}} . \quad (50)$$

However, the above expression for γ_{acc}, for fixed values of B and P, still depends on a dimensionless acceleration altitude, ζ, and therefore cannot be used in criterion (50). It is important to note that in our numerical calculations, at each altitude, we check the instant value of a particle's Lorentz factor against the above criterion. If it meets this criterion, we pick the corresponding bulk pulsar parameters such as B and P and store them as those of the death line. Generally, to make our analytic derivation of the death line self-consistent, we need an additional independent equation that relates ζ with, e.g., B and P. Obviously, the formal substitution of values of ζ_* calculated in § 2.2 into γ_{acc} in criterion (50) would lead to a trivial identity, simply because in our derivation of ζ_* we have already used the corresponding values of γ_{min}. Instead, we suggest using equations (34) and (49) to eliminate ζ to get

$$\gamma_{\text{acc}} \approx 10^7 f_{\text{prim}}B_{12}P^{-2} . \quad (51)$$

The advantage of this formula for γ_{acc} is that it does not discriminate between unsaturated and saturated regimes of acceleration of primary electrons and is factorized by the efficiency of the pulsar accelerator, f_{prim}, which may be generally regarded as a free pulsar parameter, characterizing the efficiency of primary acceleration above the pulsar PC.

Now, let us use formula (51) in criterion (50) to get explicit expressions describing the death lines for different underlying radiation mechanisms for pair-producing photons. Note that for this purpose in criterion (50) we should evaluate γ_{acc} at $f_{\text{prim}} = f_{\text{prim}}^{\text{min}}$, where $f_{\text{prim}}^{\text{min}}$ is the minimum pulsar efficiency allowing pair formation. This completes our formal definition of death lines and makes it physically sensible: for the fixed values of B and P, to specify the onset of pair formation, one needs to know the minimum energetics a primary electron beam should have to enable pair formation, i.e., one needs to know $f_{\text{prim}}^{\text{min}}$. We must note that within the framework of this approach, the analytic death lines derived in previous studies implicitly assume some fixed value for $f_{\text{prim}}^{\text{min}}$, the same for all pulsars and for all relevant pair-formation mechanisms, and that those values of $f_{\text{prim}}^{\text{min}}$ are not necessarily meaningful. On the contrary, our analytic death lines are explicitly determined by a pulsar bulk parameter $f_{\text{prim}}^{\text{min}}$. The resulting analytic death lines (or rather parameter spaces with allowed pair formation) in the P-$\dot{P}$

diagram read, for curvature radiation,

$$\log \dot{P} \geq \begin{cases} \frac{21}{8}\log P - 1.75\log f_{\rm prim}^{\rm min} - 14.6 & P \lesssim P_*^{\rm (CR)} , \\ \frac{5}{2}\log P - 2\log f_{\rm prim}^{\rm min} - 15.4 & P \gtrsim P_*^{\rm (CR)} ; \end{cases} \quad (52)$$

for resonant ICS,

$$\log \dot{P} \geq \begin{cases} \frac{5}{6}\log P - \log f_{\rm prim}^{\rm min} - 16.6 & P \lesssim P_*^{\rm (R)} , \\ \frac{2}{3}\log P - 1.33\log f_{\rm prim}^{\rm min} - 17.9 & P \gtrsim P_*^{\rm (R)} ; \end{cases} \quad (53)$$

and for nonresonant ICS,

$$\log \dot{P} \geq \begin{cases} \frac{7}{4}\log P - 1.5\log f_{\rm prim}^{\rm min} - 18.6 & P \lesssim P_*^{\rm (NR)} , \\ \frac{3}{2}\log P - 2\log f_{\rm prim}^{\rm min} - 20 & P \gtrsim P_*^{\rm (NR)} . \end{cases} \quad (54)$$

The fitting of observational data with the above expressions requires specification of the pair-producing efficiency ($f_{\rm prim}^{\rm min}$) of a pulsar PC accelerator. In this paper we calculate pulsar death lines numerically, and by comparing the analytic death lines with our numerical death lines we can estimate the values of $f_{\rm prim}^{\rm min}$ (see § 4.2.2). It is of fundamental importance to know if this value of $f_{\rm prim}^{\rm min}$ (i.e., $f_{\rm prim}$ calculated along a pair death line) is the same for all pulsars, and how it depends on the radiation process responsible for the pair formation. We find that the analytic death lines defined by equations (52)–(54) with the appropriately chosen value of $f_{\rm prim}^{\rm min}$, different for each radiation mechanism, satisfactory fit the observational data and are in a good agreement with our numerically calculated death lines. This means that our introduction of the parameter $f_{\rm prim}^{\rm min}$ and the assumption that this parameter only weakly depends on pulsar B and P values, for a given mechanism of generation of pair-producing photons, may be quite justified for the analytic tackling of pulsar death lines.

The analytic expressions above for the pair death lines differ significantly from those derived by Zhang et al. (2000). The pair death lines of Zhang et al. (2000) were derived from the condition (in our notation) that $\Delta\Phi_{\rm acc} = \Delta\Phi_{\rm max}$, which implicitly assumes that $f_{\rm prim}^{\rm min} = 1$, whereas we allow $f_{\rm prim}^{\rm min}$ to be a free parameter. As we shall see in the next section, comparison with numerical calculations implies $f_{\rm prim}^{\rm min} \ll 1$. Also, Zhang et al. (2000) computed the altitude of the PFF and thus the value of $\Delta\Phi_{\rm acc}$ from the condition $S_p(\varepsilon_{\rm min}) = S_e(\gamma_{\rm min})$, that photon attenuation length is equal to the length required for the primary electron to produce one ICS photon, since the acceleration length $S_{\rm acc} \ll S_p$. This introduced a dependence of the PFF altitude on PC temperature, which they took to be the self-consistent temperature from PC heating. By contrast, our analytic expression for the PFF altitude (eq. [7]) does not depend on PC temperature. Finally, Zhang et al. (2000) included pairs from only RICS and did not include pairs from NRICS in their ICS death lines.

4.2.2. *Comparison with Numerical Calculations*

The discussion and results of our numerical calculation of the CR and ICS pair death lines were presented in Figure 1. Since our numerical solution for the location of the PFFs are computed by iteration, we can unambiguously determine the pair death lines without having to define the efficiency, $f_{\rm prim}^{\rm min}$, as was needed in the analytic expressions above.

We must note that in our derivation of the above analytic death-line conditions we did not require the value of accelerating potential drop to be maximum at the PFF. In other words, we did not impose any ad hoc constraint on the acceleration altitude, thus making the latter consistent with the accelerating potential drop. It is remarkable that for each of the radiation mechanisms the parameter $f_{\rm prim}^{\rm min}$ (minimum efficiency of acceleration of primary beam required to set pair formation) remains nearly constant along the numerical death line. By comparing our numerically computed death lines with those given by equations (52)–(54), we find that $f_{\rm prim}^{\rm min} \sim 0.2$–0.5 for CR, 0.04–0.3 for RICS, and 0.01–0.04 for NRICS pair fronts. These efficiencies are still small compared to the maximum efficiency we estimate in the last paragraph of this section. Another important finding is that production of pairs in all observed pulsars by CR photons would require $f_{\rm prim}^{\rm min} \gg 1$, indicating the difficulty in interpreting the observational data in terms of a CR mechanism alone. On the contrary, ICS-based death lines imply much less consumption of pulsar spin-down power for pair creation. This result and our finding that the ICS-generated pairs tend to only partially screen the accelerating electric field may suggest the occurrence of "nested" pair formation regions: the lower altitude pairs produced by the ICS photons and the higher altitude pairs produced by the CR photons generated by particles accelerating through the region of the ICS pair formation.

This fact implies that if a pulsar is below the CR death line in Figure 1, and if any ICS screening is inefficient, then the primary beam acceleration is not limited by pair production and will be producing ample CR high-energy photons. The upper limit for the pulsar γ-ray luminosity in this case can be estimated by using equation (32) with the integrand evaluated at the maximum value of the potential given by equation (13) of HM98 (see also eq. [A4] of HM98):

$$L_{\gamma,\max} = c \int_{S(\eta)} \alpha(\eta)\rho(\eta,\xi)\Phi_{\max}\, dS(\eta) , \quad (55)$$

where $\Phi_{\max} \approx \frac{1}{2}[\Omega R/cf(1)]\kappa\Phi_0$, $\Phi_0 = (\Omega R/c)B_0 R$, and $dS(\eta) = S(\eta)d\Omega_\xi/\pi$, where $S(\eta)$ is the spherical cross-sectional area of the polar flux tube at radial distance r ($= \eta R$). Note that in equation (55) the integral $c\int\alpha\rho\, dS$ represents the total electron current flowing from the PC and is a constant. Thus, integrating over ξ and ϕ, we arrive at

$$L_{\gamma,\max} \approx 0.75\kappa(1-\kappa)\dot{E}_{\rm rot} \approx 0.1\dot{E}_{\rm rot} . \quad (56)$$

Here we used $\kappa = 0.15$ and $\cos\chi \approx 1$. We predict, therefore, that pulsars tend to be efficient γ-ray sources if they are to the right of their CR death lines in the B-P diagram.

4.3. *Characteristic Voltage Drop at the Pair Front*

Now we would like to demonstrate one more remarkable property of a pulsar PC accelerator. Let us take the expression for the electric potential as a function of ζ (see eq. [48]) and evaluate it at the screening altitude (at $\zeta = \zeta_*$). After substituting the corresponding expressions for ζ_* (see eqs. [36]–[38]) into equation (48), we get the following self-consistent formulae for the critical voltage drop (characteristic voltage drop at the screening altitude):

For curvature radiation,

$$\Delta\Phi_{\rm acc}(\zeta_*) = 10^{13} \text{ V} \begin{cases} 2(\tau_6/P)^{1/14} & P \lesssim P_*^{\rm (CR)} , \\ P^{-1/4} & P \gtrsim P_*^{\rm (CR)} ; \end{cases} \quad (57)$$

for resonant ICS,

$$\Delta\Phi_{\rm acc}(\zeta_*) = 10^{11} \text{ V} \begin{cases} 3(P^{-7/6}\tau_6^{1/2}) & P \lesssim P_*^{\rm (R)} \\ 2(P^{-5/4}\tau_6^{1/4}) & P \gtrsim P_*^{\rm (R)} ; \end{cases} \quad (58)$$

and for nonresonant ICS,

$$\Delta\Phi_{\rm acc}(\zeta_*) = 10^{11} \text{ V} \begin{cases} 2(P^{-1/2}\tau_6^{1/6}) & P \lesssim P_*^{\rm (NR)} , \\ P^{-3/4} & P \gtrsim P_*^{\rm (NR)} . \end{cases} \quad (59)$$

These formulae show very weak dependence of critical voltage drop on pulsar parameters B and P, especially for the CR case, as also shown by HM98. This fact simply indicates that the critical voltage drop needed for the ignition of pair formation is mainly determined by the pair-formation microphysics itself. As a result, as we move from the lower left to the upper right corner of the P-$\dot{P}$ diagram, the variation (by orders of magnitude) in the altitude of the PFF effectively compensates the corresponding change in voltage drop due to its scaling with pulsar parameters B and P, thus maintaining it near its critical value.

Note that in similar expressions derived by HA01 (see their eqs. [73]–[75]) the characteristic voltage drop varies by $\sim$4 orders of magnitude over the whole range of pulsar spin periods, $\sim$0.001–10 s.

5. POLAR CAP HEATING LUMINOSITIES AND SURFACE TEMPERATURES

5.1. *Analytic Estimates*

To estimate the efficiency of PC heating by returning positrons, we can use equations (64) and (65) of Paper I again evaluated at z_*.

Thus, setting $\kappa = 0.15$ and $\cos\chi \approx 1$, we get for the heating efficiency, $f_+ = L_+/\dot{E}_{\rm rot}$, for resonant ICS,

$$f_+^{\rm (R)} = 10^{-5}P^{-1/2}\tau_6^{3/2} \begin{cases} 2.5 & P \lesssim P_*^{\rm (R)} , \\ 1.5 & P \gtrsim P_*^{\rm (R)} ; \end{cases} \quad (60)$$

and for nonresonant ICS,

$$f_+^{\rm (NR)} = 10^{-5}P^{1/2}\tau_6 \begin{cases} 1.0 & P \lesssim P_*^{\rm (NR)} , \\ 0.6 & P \gtrsim P_*^{\rm (NR)} . \end{cases} \quad (61)$$

Here we summarize the explicit expressions for the estimated PC luminosities and surface temperatures due to the heating by positrons returning from the pair fronts set by the CR and ICS photons. Our estimates of the PC temperature are based on a standard formula $T_{\rm pc} \approx (L_+/\pi r_{\rm pc}^2 \sigma_{\rm SB})^{1/4}$, where $\sigma_{\rm SB}$ is the Stefan-Boltzmann constant. This formula therefore implies that the PC is heated homogeneously, and that the heated area is confined by the PC radius.

For curvature radiation,

$$L_+^{\rm (CR)} = 10^{31} \text{ ergs s}^{-1} \ P^{-1/2}$$
$$\times \begin{cases} 0.4\left(P^{-5/14}\tau_6^{-1/7}\right) & P \lesssim P_*^{\rm (CR)} , \\ 1.0 & P \gtrsim P_*^{\rm (CR)} , \end{cases} \quad (62)$$

$$T_{\rm pc}^{\rm (CR)} = 10^6 \text{ K } P^{-1/4} \begin{cases} P^{-5/56}\tau_6^{-1/28} & P \lesssim P_*^{\rm (CR)} \\ 2 & P \gtrsim P_*^{\rm (CR)} ; \end{cases} \quad (63)$$

for resonant ICS,

$$L_+^{\rm (R)} = 10^{28} \text{ ergs s}^{-1} \ P^{-5/2}\tau_6^{1/2} \begin{cases} 0.8 & P \lesssim P_*^{\rm (R)} , \\ 0.5 & P \gtrsim P_*^{\rm (R)} , \end{cases} \quad (64)$$

$$T_{\rm pc}^{\rm (R)} \approx 8 \times 10^3 \text{ K } P^{-9/4}\tau_6^{1/8}; \quad (65)$$

and for nonresonant ICS,

$$L_+^{\rm (NR)} = 10^{28} \text{ ergs s}^{-1} \ P^{-3/2} \begin{cases} 0.3 & P \lesssim P_*^{\rm (NR)} , \\ 0.2 & P \gtrsim P_*^{\rm (NR)} , \end{cases} \quad (66)$$

$$T_{\rm pc}^{\rm (NR)} \approx 4 \times 10^4 \text{ K } P^{-5/4} . \quad (67)$$

We caution that the above formulae are upper limits to the PC heating luminosity, in that they assume locally complete screening. As we have shown in § 3, such screening does not occur in many cases, most notably for older pulsars. Thus, as shown by the numerical calculation presented in the next section, equations (66) and (67) do not accurately predict L_+ and $T_{\rm pc}$ for millisecond pulsars, but give values that are much too high.

Let us compare the above temperature estimates with those of HA01. At $B_{12} = 1$ and $P = 0.1$ s our estimate of $T_{\rm pc}^{\rm CR}$ is roughly the same as the corresponding estimate presented by HA01 (see their eq. [58]). For the ICS cases (see their eqs. [56], [57], [59], and [60]) their estimates are systematically larger, by a factor of 3–12. However, for the millisecond pulsars we predict higher temperatures. Also, the effect that the ICS contribution to the PC temperatures dominates over the CR contribution for millisecond pulsars is more pronounced in our formulae. In addition, for long-period pulsars our formulae predict more drastic decline in the PC heating temperatures with pulsar period. We also comment that both the analytic estimates and numerical calculations of L_+ depend on the value of κ, related to the compactness and moment of inertia of the NS.

5.2. *Numerical Calculations*

We numerically evaluate the luminosity of PC heating due to ICS PFFs in a similar way to that given by equation (62) of Paper I. The fraction of returning positrons times the potential drop between the PFF and the surface is integrated in ξ across the PC. However, since in the case of ICS PFFs the potential varies significantly across the width of the PFF, we also integrate the product of the potential and the returning positron fraction at each altitude between
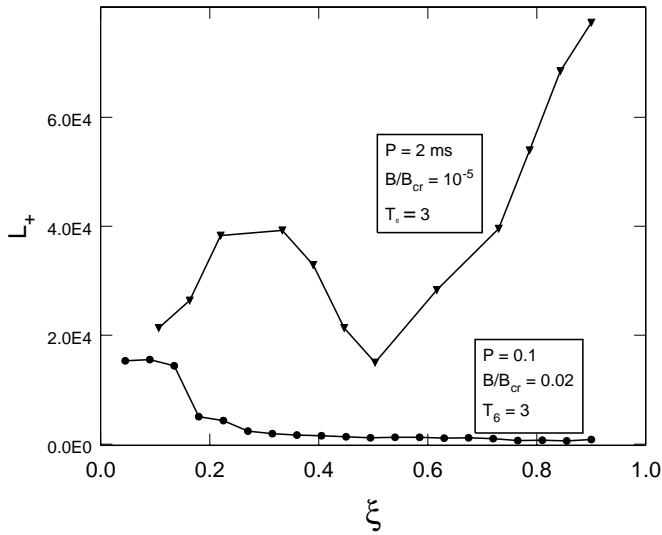
FIG. 7.—Examples of the variation of PC heating luminosity, L_+, as a function of magnetic colatitude, ξ, in units of the PC half-angle.

z_0 and $z_0 + \Delta_s$:

$$L_+ = 2\alpha c S_{pc} \eta_0^3 \frac{f(1)}{f(\eta_0)} \int_0^1 \int_{z_0}^{z_0+\Delta_s} \rho_+(z - z_0, \xi) \Phi(z, \xi) \, dz \, \xi \, d\xi$$

$$= \int_0^1 L_+(\xi) \, \xi \, d\xi \,, \qquad\qquad (68)$$

where $S_{pc} = \pi \Omega R^3 / cf(1)$ is the area of the PC. Figure 7 shows the dependence of $L_+(\xi)$ on ξ, which reflects the distribution of heating across the PC. Most of the PC heating due to the ICS pair front occurs at small ξ, near the magnetic pole for normal pulsars, but in the outer part of the PC for millisecond pulsars.

The total positron heating luminosity, scaled with the spin-down luminosity, as a function of characteristic pulsar age, $\tau = P/2\dot{P}$ is shown in Figure 8 for two different values of PC temperature. The numerically computed $L_+/\dot{E}_{rot}$

increases with τ, in agreement with the analytic estimate (eqs. [60] and [61]), as long as there is locally complete screening. When complete screening is no longer achieved, at a τ value that depends on P and T_6, the heating rate saturates because the number of pairs produced is not sufficient to return a positron flux proportional to z_0. Even at very high PC temperatures, the millisecond pulsars have reached saturation of the PC heating rate because they are beyond the ICS screening boundary. The heating luminosity is larger for a lower value of T_6 before saturation because the PFF is at higher altitude and the potential drop is higher, giving the positrons more energy before they reach the NS surface. Figure 9 displays the same calculations of the PC heating luminosity, not scaled to the spin-down luminosity, to more easily compare with observations. In these figures we have also plotted for comparison the calculations of PC heating luminosity from the CR PFFs presented in Paper I. The high-τ end of the CR heating rate curves marks the CR PFF pair death line for that period. Where heating from positrons returning from the CR PFF is present, it is several orders of magnitude larger than the heating from the ICS PFF, so that in these pulsars heating from the ICS pairs makes a negligible contribution to the total PC heating rate. For normal pulsars, heating from ICS pair fronts is not high enough to be detectable at present, even in the absence of CR pair heating. However, emission from ICS pairs provides the only source of PC heating for the known millisecond pulsars, which have ages of $\tau > 10^8$ yr, since they cannot produce CR pairs. This emission may be detectable if the PC temperatures are above 10^6 K. The relatively high ICS pair heating rates in the millisecond pulsars are due primarily to the higher voltage drop necessary to make pairs. Even though the fraction of returning positrons is not large, the positrons gain more energy before hitting the NS surface.

The analytic estimates for L_+ are in reasonably good agreement with our numerical calculations (within a factor of 10) in the regime where locally complete screening is occurring. Where complete screening is not achieved, the analytic estimates of L_+ and also of T_{pc} given in § 5.1 will
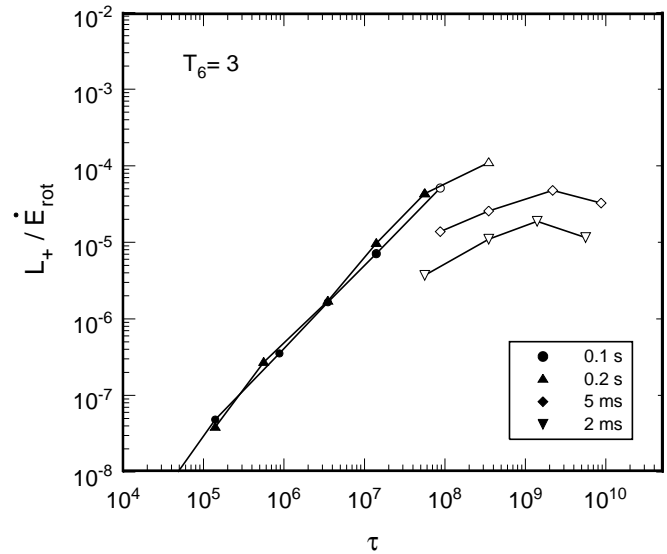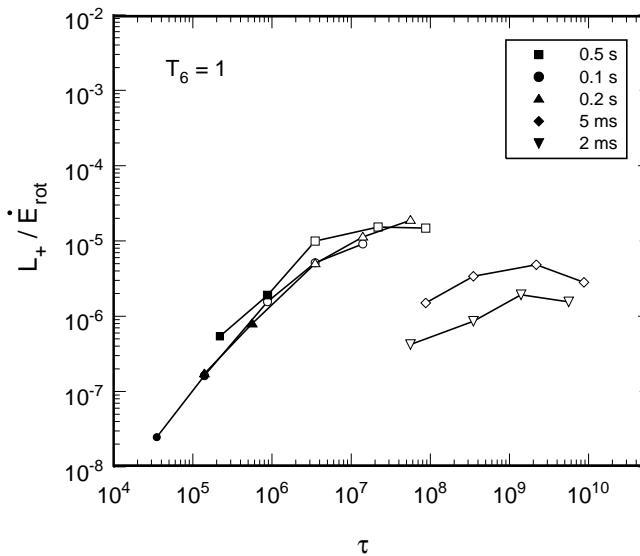

FIG. 8.—PC heating luminosity from ICS pair fronts, L_+, normalized to the spin-down energy-loss rate, $\dot{E}_{rot}$, as a function of the characteristic spin-down age, $\tau = P/2\dot{P}$, for different pulsar periods, as labeled, and PC temperature (a) $T_6 = 1.0$ and (b) $T_6 = 3.0$. Filled symbols designate locally complete screening, and open symbols indicate that no screening occurs above the ICS pair front.
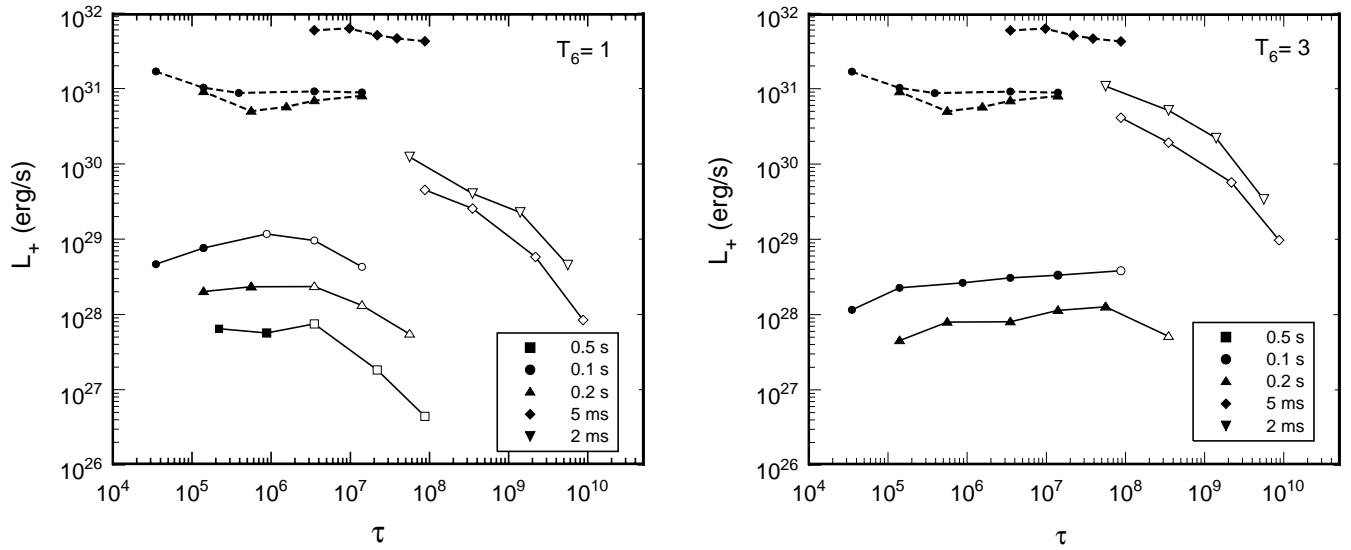
FIG. 9.—PC heating luminosity, L_+, as a function of the characteristic spin-down age, $\tau = P/2\dot{P}$, for different pulsar periods, as labeled, and PC temperature (a) $T_6 = 1.0$ and (b) $T_6 = 3.0$. Solid curves show heating luminosities from ICS pair fronts and dashed curves show heating luminosities from CR pair fronts (from Paper I). Filled symbols designate locally complete screening, and open symbols indicate that no screening occurs above the ICS pair front.

greatly overestimate the true values. This is especially true in the case of the millisecond pulsars. We caution that equations (64)–(67) cannot be used for pulsars that are beyond the screening boundaries of Figure 4.

In Figure 10, we show the predicted luminosities from ICS PC heating, L_+ as a function of PC surface temperature (*solid lines*) for two different pulsar periods and a surface field of $B_0 = 4.4 \times 10^8$ G, so that the corresponding characteristic ages would be $\tau = 1.4 \times 10^9$ yr for $P = 2$ ms and $\tau = 8.75 \times 10^9$ yr for $P = 5$ ms. There is a definite dependence $L_+ \propto T^2$ seen in these curves, which cannot be modeled analytically since these cases do not have full screening. Also plotted (*dashed lines*) are the luminosities, $L_{BB} = A\sigma_{SB}T^4$, emitted by a blackbody at PC radiating temperature T and different heated surface areas A. The intersections of the curves roughly indicate values of tem-

perature at which self-sustained heating (i.e., where the surface emission at a given temperature supplies just enough returning positrons from ICS pairs to maintain the PC at that temperature) is possible for heated PCs of a particular area. Since the standard PC area is $A_{pc} = 3.3 \times 10^{11}$ cm^2 for $P = 2$ ms and $A_{pc} = 1.3 \times 10^{11}$ cm^2 for $P = 5$ ms, self-sustained PC heating emission requires heated and radiating areas much smaller than the entire PC area. The intersection points of the blackbody and L_+ curves in Figure 10 are not entirely self-consistent self-sustained heating models, since we assume a radiating area of A_{pc} for our calculations. The fully self-consistent models would have radiating areas somewhat larger at a given temperature, but still smaller than A_{pc}.

Of the six millisecond radio pulsars that have been detected as pulsed X-ray sources, most have narrow pulses and power-law spectra, indicating that their emission is dominated by nonthermal radiation processes. However, two pulsars, PSR J0437−4715 ($P = 5.75$ ms, $\tau = 4.6 \times 10^9$ yr) and PSR J2124−3358 ($P = 4.93$ ms, $\tau = 7.3 \times 10^9$ yr), have possible thermal emission components, which would imply that some surface heating is taking place. The emission from PSR J0437−4715 has a dominant power-law component, but a two-component model is required for an acceptable fit. A two-component power-law plus blackbody fit to combined *Extreme Ultraviolet Explorer* (*EUVE*) and *ROSAT* data (Halpern, Martin, & Marshall 1996) give a temperature of $T = (1.0–3.3) \times 10^6$ K, luminosity $L = 8.4 \times 10^{29}$ ergs s^{-1}, and emitting area $A = 7.8 \times 10^7$–1.1×10^{10} cm^2 for the thermal component. Recent *Chandra* observations of PSR J0437−4715 (Zavlin et al. 2001) confirm that at least one thermal component plus a power law is needed to fit the spectrum. Their preferred model consists of a two-temperature thermal blackbody, with a hotter PC core of $T_{core} = 2.1 \times 10^6$ K and $R_{core} = 0.12$ km and a cooler PC rim of $T_{rim} = 5.4 \times 10^5$ K and $R_{rim} = 2.0$ km. A blackbody fit to *ASCA* emission from PSR J2124−3358 (Sakurai et al. 2001) yields a temperature $3.6^{+0.93}_{-0.70} \times 10^6$ K, luminosity $L = 4.8 \times 10^{29}$ ergs s^{-1}, and PC emitting area $A = 1.4^{+2.5}_{-0.9} \times 10^7$ cm^2.
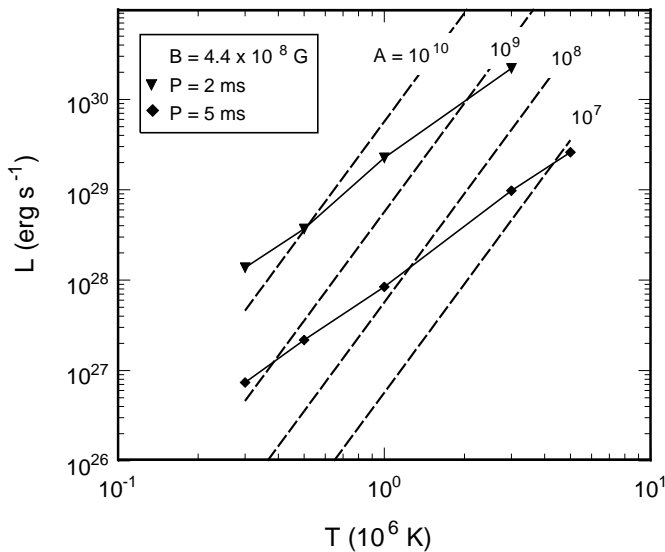

FIG. 10.—PC heating luminosity L_+ (*solid curves*) for different pulsar periods, as labeled, and blackbody luminosity $L_{BB} = A\sigma_{SB}T^4$ for different areas A in cm^2, as labeled, as a function of PC temperature, T.

Comparing our results in Figure 10 with the observed values of T, L, and A for PSR J0437−4715 and PSR J2124−3358, we see that the predicted luminosities, areas, and temperatures for self-sustained PC heating are in a range comparable to observed values. Thus, ICS pair fronts could be a plausible source of PC heating for some millisecond pulsars.

Recent *Chandra* high-resolution X-ray observations of the Galactic globular cluster 47 Tuc (Grindlay et al. 2001) have detected all 15 known ms radio pulsars in the cluster as well as a number of other suspected millisecond pulsars. It is thought that the X-ray source population of 47 Tuc is dominated by millisecond pulsars having soft spectra and luminosities $L_X \sim 10^{30}$ ergs s^{-1}. Grindlay et al. (2002) have found a dependence $\log L_X = -(0.32 \pm 0.1) \log \tau + 33.3$ for the millisecond pulsars in the cluster, not too different from what we have found for PC heating from ICS pair fronts (cf. Fig. 9b).

6. SUMMARY AND CONCLUSIONS

We have explored production of electron-positron pairs by photons produced through ICS of thermal X-rays by accelerated electrons above a pulsar PC. Since the accelerating primary electrons can produce pairs from ICS photons at much lower energies than are required to produce pairs from CR photons, it is very important to investigate the consequences of ICS pair fronts for $E_\parallel$ screening and for PC heating. We have defined "pair death" lines in B_0-P space as the boundary of pair production for pulsars, having dipole magnetic fields of surface strength $6.4 \times 10^{19}(\dot{P}P)^{1/2}$ G. Operationally, the existence of a pair front is determined by a finite solution to equation (7) for S_0, the altitude of the onset of pair creation. Although we are able to give analytic formulae for the altitude of the PFFs for different radiation processes, the location of the pair death lines must be determined numerically. The existence of a pair front requires much less than one pair per primary electron (but still many pairs from the whole PC beam), since the very first pairs are created in the declining high-energy tail of the radiated spectrum, and also much less than the number of pairs per primary required for screening of $E_\parallel$. We find that virtually all known radio pulsars are capable of producing pair fronts with ICS photons. A smaller number, less than half, are also able to produce pairs via CR. If the acceleration model we use is correct and pulsars have dipole fields, then this result implies that relatively few pairs are required for coherent radio emission.

Self-consistent calculations show that ICS pair fronts produce lower fluxes of returning positrons and lower PC heating luminosities than CR pair fronts. This is due to the higher efficiency of the ICS process in producing pairs at lower altitudes where both the charge deficit required to screen (and thus the returning positron flux) and the accelerating voltage drop are smaller. For pulsars with surface magnetic fields in the "normal" range of 10^{11}–10^{13} G, ICS heating luminosities are several orders of magnitude lower than CR heating luminosities. However, for millisecond pulsars having surface fields in the range 10^8–10^{10} G, production of any pairs requires such high photon energies that ICS pair fronts occur at higher altitudes, where acceleration voltage drops are high enough to produce significantly more PC heating. Since most millisecond pulsars cannot produce pairs through CR, ICS pair fronts provide the only means

of external PC heating. We find that for surface temperatures $T \gtrsim 10^6$ K, ICS heating luminosities are in the range of detection.

We find that ICS pairs are able to screen the *local* $E_\parallel$ in some pulsars having a high enough PC temperature, but that this local screening will not produce a complete screening of the accelerating field at all altitudes and thus will not stop the acceleration of the primary beam. This is because the number of ICS pairs grows slowly, on a scale length comparable to the altitude of the PFF, and then declines, while the charge deficit that maintains $E_\parallel$ continues to increase with altitude. Even if the ICS pair production is vigorous enough to achieve local screening of $E_\parallel$, it eventually cannot produce the charge density (from returning positrons) to keep up with the increasing charge deficit (produced by the combination of flaring field lines and inertial frame-dragging). The primary particles may slow their acceleration briefly, as a result of the local screening, but will resume acceleration once the ICS pair production declines. At higher altitudes, those pulsars to the left of the CR pair death line will reach the Lorentz factors ($\gamma \sim 2 \times 10^7$) required to produce CR pairs. In contrast to ICS pair fronts, the growth of pairs above the CR PFF is rapid and robust because of the sensitivity of CR photon energy and emission rate on particle Lorentz factor, producing complete screening of $E_\parallel$ in a very short distance (cf. Paper I). In pulsars to the right of the CR pair death line, there is not complete screening and the primary particles will continue accelerating to high altitude, with their Lorentz factor being possibly limited by CR reaction.

We have also investigated the proposal by HM98 that pairs produced as the returning positrons are accelerated toward the NS may be able to screen the $E_\parallel$ above the surface. Using our calculated values of the returning positron flux in cases where local screening has been achieved at the ICS pair fronts, we find that in most cases screening does not occur at a significant distance above the NS surface to cause disruption of a steady state or formation of pair fronts. In the cases where screening does occur near PFFs significantly above the surface, the pulsars are near the ICS screening boundary. The resulting instability would then not move the start of the acceleration to higher altitudes, as HM98 had envisioned, but would probably weaken or disrupt the screening at the upper ICS pair front, resulting in a decrease in returning positron flux, which would weaken the screening at the lower PFF, etc.

PC heating by CR pair fronts will dominate for pulsars to the left of the CR pair death line, while ICS pair fronts will supply the PC heating for pulsars to the right of the CR pair death line. While we have given analytic expressions for the fraction of returning positrons and PC heating luminosities from ICS pair fronts, these are only good estimates above the ICS screening boundaries of Figure 4. Below the ICS screening boundaries, where local screening is not achieved for that PC temperature, the numerical values of returning positron fraction and heating luminosity fall well below the analytic estimates. This will be true for millisecond pulsars, nearly all of which are below the ICS screening boundary for a PC temperature of even $T = 10^7$ K.

Our results are dependent on a number of assumptions inherent in our calculations. First, we have assumed that the pattern of thermal X-ray emission is from a heated PC and is a pure, isotropic blackbody. According to recent calculations (Zavlin et al. 1995) of radiation transfer in magnetized

NS atmospheres, the thermal emission is not pure blackbody or isotropic, but a somewhat cooler blackbody consisting of pencil and fan beam components. Both effects of full surface (cooler) emission and pencil beaming would tend to decrease ICS radiation and thus ICS pair production efficiency. However, a large fan beam component would tend to increase ICS efficiency. Second, we have used a hybrid scheme to describe the ICS radiation spectrum in which the RICS has been treated as classical magnetic Thompson scattering and NR (or continuum) ICS has been treated as relativistic but nonmagnetic. In reality, both RICS and NRICS should be treated as a single process with one cross section. While the magnetic QED scattering cross section has been studied for some time (e.g., Herold 1979; Daugherty & Harding 1986), simple expressions in limited cases are only beginning to become available (e.g., Gonthier et al. 2000). Our present treatment is probably accurate for magnetic fields $B \lesssim 0.2 B_{\mathrm{cr}}$, which includes most of the radio pulsars.

The location of a pulsar relative to the pair death lines may be important not only to its radio and thermal X-ray emission characteristics, but also to its high-energy emission properties. As we have argued in this paper, ICS pair fronts will not limit the acceleration voltage drop in pulsars, but that acceleration will continue until it is limited by a CR pair front. The voltage drop at the CR pair front (together with the size of the PC current) is therefore expected to determine the high-energy emission luminosity. In § 4, we have noted that the acceleration voltage drop of pulsars that produce CR pair fronts is remarkably insensitive to pulsar parameters, leading to the prediction that high-energy luminosity, L_{HE}, should be simply proportional to PC current (which is proportional to $\dot{E}_{\mathrm{rot}}^{1/2}$), which seems to be borne out by observations (e.g., Thompson 2000). However, pulsars that do not produce CR pair fronts do not have such a limit on acceleration voltage drop and should depart from the $L_{\mathrm{HE}} \propto \dot{E}_{\mathrm{rot}}^{1/2}$ dependence, and approach a $L_{\mathrm{HE}} \propto \dot{E}_{\mathrm{rot}}$ dependence. Indeed, such a departure must occur if they are not to exceed 100% efficiency in converting rotational energy loss to high-energy emission. We predict that this change in L_{HE} dependence should occur along the CR pair death line. None of the pulsars that have detected γ-ray emission are to the right of the CR pair death line, although some, such as Geminga, are close. The *Large Area Gamma-Ray Telescope* (*GLAST*) will have the sensitivity to detect γ-ray emission from significant numbers of radio pulsars beyond the CR pair death line and so should be able to test this prediction.

REFERENCES

Arons, J. 1981, ApJ, 248, 1099
———. 1998, in Neutron Stars and Pulsars, ed. N. Shibazaki et al. (Tokyo: Univ. Academy Press), 339
Arons, J., & Scharlemann, E. T. 1979, ApJ, 231, 854
Baring, M., & Harding, A. K. 2001, ApJ, 547, 929
Chen, K., & Ruderman, M. 1993, ApJ, 402, 264
Daugherty, J. K., & Harding, A. K. 1986, ApJ, 309, 362
Dermer, C. 1990, ApJ, 360, 197
Gonthier, P. L., Harding, A. K., Baring, M. G., Costello, R. M., & Mercer, C. L. 2000, ApJ, 540, 907
Grindlay, J. E., Camilo, F., Heinke, C., Edmonds, P. D., Cohn, H., & Lugger, P. 2002, ApJ, submitted
Grindlay, J. E., Heinke, C., Edmonds, P. D., & Murray, S. S. 2001, Science, 292, 2290
Halpern, J. P., Martin, C., & Marshall, H. L. 1996, ApJ, 462, 908
Harding, A. K., Baring, M. G., & Gonthier, P. L. 1997, ApJ, 476, 246
Harding, A. K., & Muslimov, A. G. 1998, ApJ, 508, 328 (HM98)
———. 2001, ApJ, 556, 987 (Paper I)

Harding, A. K., & Preece, R. D. 1987, ApJ, 319, 939
Herold, H. 1979, Phys. Rev. D, 19, 2868
Hibschman, J. A., & Arons, J. 2001, ApJ, 554, 624 (HA01)
Jones, F. 1968, Phys. Rev., 167, 1159
Manchester, R. N., et al. 2001, MNRAS, in press
Muslimov, A. G., & Tsygan, A. I. 1992, MNRAS, 255, 61 (MT92)
Ruderman, M., & Sutherland, P. G. 1975, ApJ, 196, 51
Sakurai, I., et al. 2001, PASJ, 53, 535
Sturrock, P. 1971, ApJ, 164, 529
Tademaru, E. 1973, ApJ, 183, 625
Thompson, D. J. 2000, in High Energy Gamma-Ray Astronomy, ed. F. A. Aharonian & H. J. Volk (AIP: New York), 103
Zavlin, V. E., Pavlov, G. G., Shibanov, Yu. A., & Ventura, J. 1995, A&A, 297, 441
Zavlin, V. E., et al. 2001, ApJ, submitted
Zhang, B., & Harding, A. K. 2000, ApJ, 532, 1150
Zhang, B., Harding, A. K., & Muslimov, A. G. 2000, ApJ, 531, L135
Zhang, B., Qiao, G. J., Lin, W. P., & Han, J. L. 1997, ApJ, 478, 313